

A Novel Deep Hybrid Framework with Ensemble-Based Feature Optimization for Robust Real-Time Human Activity Recognition

Wasi Ullah^{1,2}, Yasir Noman Khalid¹, Saddam Hussain Khan²,

¹Department of Computer Science, HITEC University, Museum Road, Taxila, Pakistan

²Department of Computer Systems Engineering, UEAS, Swat, Pakistan

Email: wasi.ullah@student.hitecuni.edu.pk

Abstract

Human Activity Recognition (HAR) plays a pivotal role in various applications, including smart surveillance, healthcare, assistive technologies, sports analytics, etc. However, HAR systems still face critical challenges, including high computational costs, redundant features, and limited scalability in real-time scenarios. An optimized hybrid deep learning framework is introduced that integrates a customized InceptionV3, an Attention-Augmented AA-LSTM architecture, and a novel ensemble-based feature selection strategy. The proposed framework first extracts spatial descriptors using the customized InceptionV3 model, which captures multilevel contextual patterns, region homogeneity, and fine-grained localization cues. The temporal dependencies across frames are then modeled using AA-LSTMs to effectively encode motion dynamics. Finally, an ensemble-based genetic algorithm with Adaptive Dynamic Fitness Sharing and Attention (ADFSA) is employed to select a compact and optimized feature set by dynamically balancing objectives such as accuracy, redundancy, uniqueness, and complexity reduction. Consequently, the selected feature subsets, which are both diverse and discriminative, enable various lightweight machine learning classifiers to achieve accurate and robust HAR in heterogeneous environments. Experimental results on the robust UCF-YouTube dataset, which presents challenges such as occlusion, cluttered backgrounds, motion dynamics, and poor illumination, demonstrate good performance. The proposed framework achieves 99.65% recognition accuracy, reduces features to as few as 7, and enhances inference time. The lightweight and scalable nature of the HAR system supports real-time deployment on edge devices such as Raspberry Pi, enabling practical applications in intelligent, resource-aware environments, including public safety, assistive technology, and autonomous monitoring systems.

Keywords: Human Activity Recognition, Hybrid Deep Learning, InceptionV3, LSTM Networks, Ensemble Feature Selection, Adaptive Dynamic Fitness Sharing, Real-Time Processing, Edge Computing

1 Introduction

Human activity recognition (HAR) plays a pivotal role in the development of smart cities, particularly in the context of video-based surveillance. Accurate identification of human behavior can help law enforcement and public safety agencies detect irregular activities ranging from accidents and property damage to illicit behaviors such as fighting and theft. Early research in HAR focused primarily on controlled environments with a single actor, but recent studies have shifted toward more realistic and challenging scenarios. These include uncontrolled video datasets with complex backgrounds, varying illumination, camera movement, and occlusion, making accurate recognition considerably more difficult [1]. Improving pedestrian detection and tracking in such dynamic surveillance situations remains a significant challenge.

Although Convolutional Neural Networks (CNNs) have demonstrated remarkable performance in image classification and object detection, they are inherently limited to processing individual frames. They cannot directly capture temporal dynamics in video sequences [2]. To address this, two-stream CNNs were presented, in which appearance and motion information (e.g., optical flow) are processed separately. Although they achieve good recognition performance, they incur high computational costs, limiting their suitability for large-scale or real-time applications [3, 4]. More recently, 3D CNNs have been introduced to directly extract spatiotemporal information from raw video streams [5, 6]. To enhance temporal modeling, recurrent architectures such as RNNs and LSTMs have also been incorporated [7, 8]. These approaches suffer from high computational cost, especially when processing long video sequences, which limits their applicability for large-scale and real-time scenarios.

Recently, Transformer-based models have become popular in human activity recognition. For video data, researchers have combined 3D convolution with attention-based Transformers to better capture both spatial and temporal patterns, while efficiency-focused architectures have enabled lightweight, real-time processing in open-set HAR tasks [9, 10]. In the wearable sensor domain, methods like MoPFormer, SETransformer, and P2LHAP have introduced novel innovations, including tokenization into motion primitives, channel-wise attention, and sequence forecasting, achieving improved accuracy, interpretability, and generalization across datasets [11, 12]. Lightweight, end-to-end Transformers for smartphone IMU data also match or exceed CNN–LSTM baselines with fewer parameters and strong performance [13]. Despite these gains, recent surveys note that Transformer models often entail heavy computation, dependency on large datasets, and limitations when deployed on resource-constrained devices, posing challenges to their broader adoption [14].

To address these limitations, researchers have explored feature fusion and selection strategies for HAR. Promising performance achieved by incorporating deep spatial and motion representations using spatial–temporal attention mechanisms [15] and combining hand-crafted multi-view features with feature selection (FS) based on entropy variability [16]. They often rely on hand-crafted components and produce high-dimensional feature representations, leading to increased computational complexity and limited scalability. Efficient selection of discriminative features is therefore essential to improve inference speed without compromising accuracy.

In this work, we propose a novel hybrid HAR framework that integrates a customized InceptionV3 CNN for spatial feature extraction with an Attention-Augmented (AA-LSTM) network for temporal modeling. The CNN captures discriminative spatial patterns from individual frames, while the AA-LSTM models temporal dependencies across sequences. Designed for real-time video processing, the framework handles challenges such as occlusion, cluttered backgrounds, motion blur, and multiview variations, as exemplified by the UCF YouTube action dataset [17]. Both models are end-to-end trainable and optimized via transfer learning and fine-tuning to ensure efficient inference. Furthermore, to reduce feature redundancy and computational overhead, a genetic algorithm (GA)–based FS strategy is applied, selecting only the most discriminative spatiotemporal features for final classification. By eliminating the need for costly preprocessing steps such as optical flow or skeleton extraction, the proposed framework achieves high accuracy while maintaining practical real-time applicability.

The following are the main contributions of this work:

- This study proposes a hybrid DL framework that synergistically integrates spatial customized InceptionV3 and temporal AA-LSTM modeling for HAR from video data. The customized InceptionV3 integrates region-based (average pooling) and boundary-aware (max pooling) operations after each convolutional block to enhance region homogeneity, suppress noise, and capture discriminative local features, while improving robustness through down-sampling. Moreover, the enhanced InceptionV3 extracts fine-grained localization, contextual cues, and human positioning within frames, which an AA-LSTM sequentially processes to model inter-frame temporal dependencies and motion dynamics with high fidelity.
- A novel ensemble-based GA-driven FS strategy, ADFSFA, is employed to achieve compact and discriminative feature subsets. The ADFSFA mechanism dynamically reweights multiple objectives:

classification accuracy, redundancy minimization, uniqueness enhancement, and complexity reduction through attention-guided adaptation, thereby accelerating convergence and mitigating local stagnation during the evolutionary process.

- The optimally selected and diverse feature subsets include both spatial and temporal, are highly compact, diverse, and discriminative, enabling lightweight ML classifiers to achieve robust HAR performance across heterogeneous conditions with minimal resource overhead.
- The proposed framework outperforms state-of-the-art approaches on the UCF–YouTube dataset with 99.65% recognition accuracy, while reducing the feature space from 128 to 7. This compact representation enables real-time inference on edge devices such as a Raspberry Pi. .

The rest of the paper is organized as follows. Section II provides related work. Section III presents the methodology and proposes the ADFSFA scheme. Section IV is related to the experimental setup. Results and discussion are elaborated in section V. Section VI concludes the paper.

2 Related Work

Recent research has increasingly emphasized advanced DL architectures for HAR, spanning CNN-based frameworks, transfer learning paradigms, and, more recently, Transformer-driven sequence modeling. The BT-LSTM model [18], for instance, achieved 85.3% accuracy on the UCF11 dataset, highlighting the importance of temporal modeling but exhibiting limited generalization in unconstrained scenarios. To jointly capture spatial and temporal dependencies, several end-to-end architectures have been explored. The CNN–BiLSTM framework [19] attained 92.84% accuracy, while the deep autoencoder–CNN approach [20] reached 96.2%. However, these models required large-scale training data and involved substantial computational costs, reducing their feasibility in real-time applications.

Efforts to strengthen spatial representation also included handcrafted and hybrid descriptors. The key-frame driven KFDI method [21] achieved only 79.4%, largely due to weak spatial discrimination. More sophisticated designs, such as the dilated CNN–BiLSTM with residual blocks [22] and the local–global feature fusion with QSVM [23], achieved 89.01% and 82.6%, respectively. However, these methods exhibited reduced robustness when applied to complex activities with occlusions, cluttered backgrounds, and motion variations.

More recently, fully 3D CNN and Transformer-based encoders have been introduced to address long-term temporal modeling. The 3D-CNN [24] reported 85.20% accuracy, whereas the ConvNeXt–TCN framework [25] achieved 97.73%, underscoring the role of temporal aggregation. Hybrid architectures such as VGG–BiGRU [26] and ViT–ReT [27] attained 93.38% and 92.4% accuracy, respectively. However, despite these advancements, most of these models employed parameter-heavy architectures and retained high-dimensional feature representations, resulting in increased inference latency and limited applicability on resource-constrained platforms.

Additionally, the bidirectional LSTM model [28] reported a high recognition accuracy of 99.2%, yet it relied on full feature vectors without any dimensionality reduction. This dependence on high-dimensional features limited its scalability and efficiency in real-time or edge-deployment environments. Overall, prior studies have demonstrated significant progress but continue to face challenges related to computational efficiency, redundancy in feature representation, and deployment feasibility. A concise summary of existing approaches is presented in Table 1.

Despite notable progress, existing HAR models still face challenges related to computational efficiency, redundancy in feature representation, and deployment feasibility on real-time or edge platforms. This highlights the need for lightweight yet effective frameworks that can balance recognition accuracy with scalability and efficiency. To overcome these shortcomings, this study proposes a novel deep hybrid framework with ensemble ADFSFA FS scheme. The method integrates multiple optimization objectives, including accuracy, redundancy, uniqueness, and complexity, that dynamically adjust their relative importance throughout the evolutionary process. Additionally, by leveraging a two-stage deep feature extraction pipeline (customized InceptionV3 + AA-LSTM), the method effectively captures

Table 1. Summary of Previous Works on Human Activity Recognition

Ref.	Dataset(s)	Results / Method	Key Shortcomings
[18]	UCF11, KTH	Block-term tensor RNN; 94% (UCF11)	Requires tensor decomposition + full RNN; high computation
[19]	UCF11, KTH	CNN features + BiLSTM; 94.9%	No feature reduction → high-dimensional inputs → slower inference
[20]	UCF11, surveillance	Deep autoencoder + CNN; 93.6%	Lacks explicit temporal modeling; not optimized for real-time
[21]	UCF11	Dynamic Image + CNN; 95.7%	Ignores temporal sequences → limited spatio-temporal modeling
[22]	UCF11, HMDB51, UCF50	Dilated CNN + Attention-LSTM; 96.5% (UCF11)	Heavy attention block; poor generalization (68.4% HMDB51)
[23]	EUCF-11 / RUCF-11	Spiking CNN for event data; 92.5% / 95.7%	Designed for neuromorphic data, not RGB video; no feature reduction
[24]	UCF101	3D-CNN; 94.1%	High memory and inference time due to 3D convolutions
[25]	UCF11, UCF50, UCF101, JHMDB	ConvNeXt + TCN; 97.73%, 98.81%, 98.46%, 83.38%	Very accurate, but deep/heavy model; no feature compression
[26]	UCF Sports, JHMDB, UCF101	CNN + BiGRU + FS; 95.2%, 78.7%, 93.4%	Features still high-dimensional; no real-time deployment
[27]	UCF101, HMDB51	ViT-ReT; 97.4%, 82.6%	Transformer complexity; high inference cost
[28]	UCF11, JHMDB	TL + BiLSTM; 96.7%, 79.5%	Uses full feature vectors; no dimensionality reduction

both spatial and temporal representations. This hybrid design enables the proposed framework to achieve better recognition performance, faster inference, and reduced model complexity, making it well-suited for real-time HAR applications.

3 Methodology

This study presents a novel hybrid deep feature extraction and selection framework for HAR, structured into four sequential phases:

1. **Data Preprocessing:** Video data is decomposed into frames, uniformly sampled, resized to 224×224 pixels, normalized, and augmented through controlled transformations to enhance robustness and mitigate overfitting.
2. **Spatial Feature Extraction:** A customized InceptionV3 captures fine-grained spatial descriptors, including contextual cues, region homogeneity, and discriminative local patterns.
3. **Temporal Modeling:** An AA-LSTM encodes inter-frame dependencies and motion dynamics with high temporal fidelity.
4. **Feature Selection and Classification:** An ensemble-based genetic algorithm with ADFSFA identifies compact, non-redundant, and highly discriminative feature subsets, which are subsequently classified using lightweight machine learning models.

This phased pipeline shown in Figure 1, ensures a balance between accuracy, compactness, and computational efficiency, supporting real-time deployment on edge devices. The framework is further benchmarked against state-of-the-art methods to validate its effectiveness.

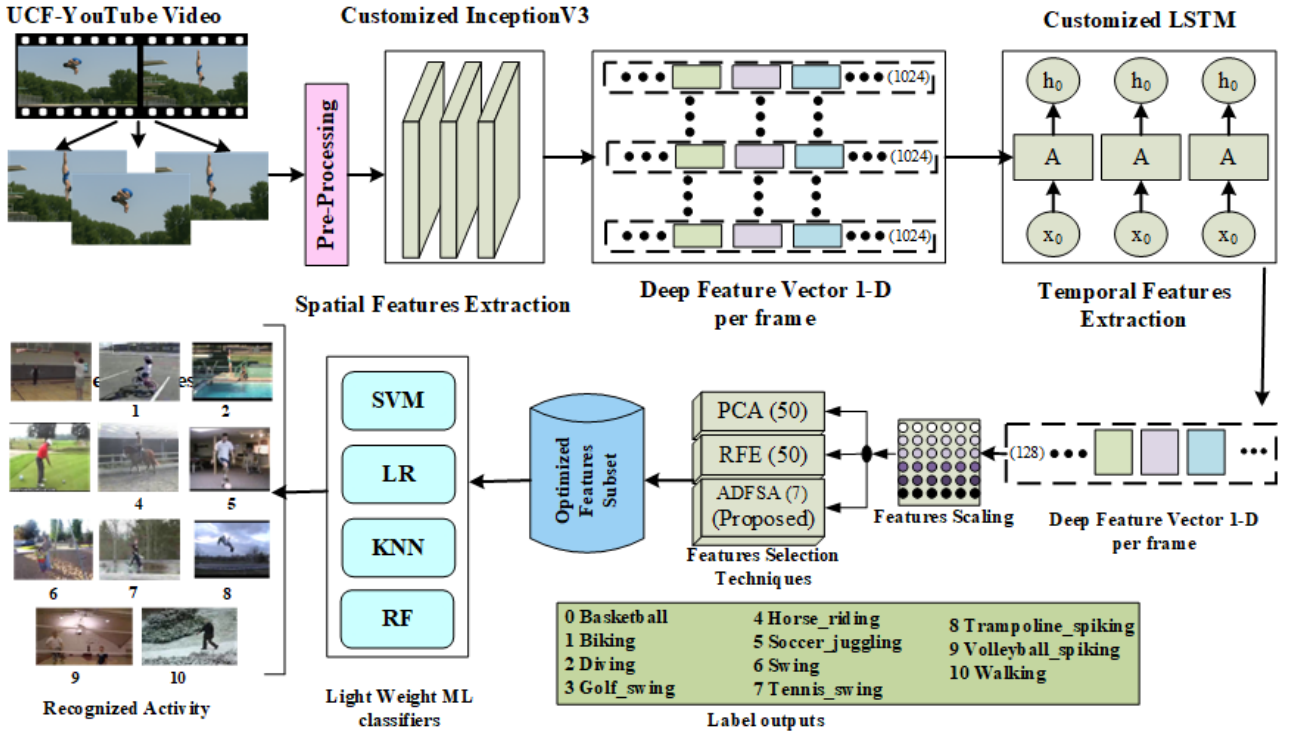


Figure 1. Overall Block Diagram of Proposed Framework.

3.1 Data Preprocessing

3.1.1 Frames Extraction from Video Clip

As deep CNN operate on image data, it is essential to extract individual frames from the video stream. To achieve this, a windowing mechanism is employed, which determines the interval at which frames

are sampled and stored. This interval, referred to as the skip window size or sampling interval, is calculated using the following formula:

$$window_size = \max \left(\frac{video_frames_count}{Sequence_Length} \right). \quad (1)$$

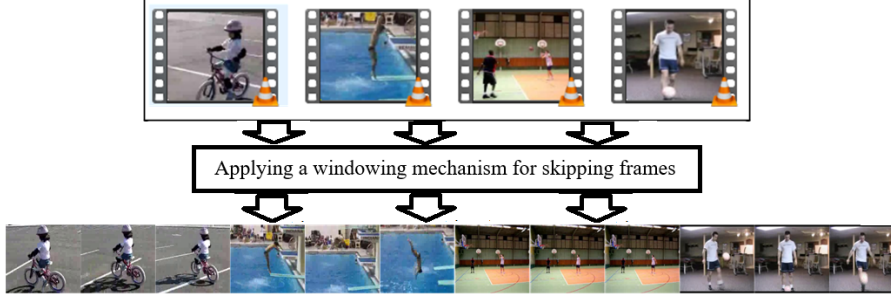


Figure 2. Video to Frames Extraction.

Initially, video data should undergo a frame extraction process, where individual frames are captured at a predetermined rate and resolution, as illustrated in Figure 2, in order to obtain a collection of images with uniform characteristics throughout the dataset.

3.1.2 Image resizing

In this study, image preprocessing is applied to align the input dimensions of video frames with the expected input format of the modified deep convolutional architecture. Each frame is resized to 224×224 pixels with 3 color channels (RGB), ensuring compatibility with the customized Inception-based feature extractor. Alongside resizing, pixel intensities are normalized to a fixed scale, typically in the range $[0, 1]$, or standardized using the appropriate preprocessing function. This step harmonizes the input distribution with that of the network’s training conditions, promoting stable convergence and effective spatial feature extraction from each frame in the sequence.

3.1.3 Data Augmentation

To enhance the diversity and generalization of the model, data augmentation techniques are applied during the preprocessing phase. These augmentations simulate real-world variations and prevent overfitting by introducing randomness into the training data [29]. Common transformations include random horizontal flipping, slight rotations, zooming, and brightness adjustments, all applied within controlled bounds to preserve the semantic content of human activities. These augmentations are executed on a per-frame basis before the frames are fed into the feature extractor. By increasing variability in spatial patterns without altering temporal coherence, data augmentation enhances the robustness and reliability of temporal feature learning in downstream AA-LSTM-based modeling.

3.2 Feature Extraction via Deep Hybrid Convolutional Neural Network

This paper proposes a deep hybrid architecture that combines a customized InceptionV3 model with an AA-LSTM network for effective human activity recognition. The inception-V3 model is employed to extract rich spatial features from individual video frames, while the AA-LSTM network captures the temporal dependencies across frame sequences. This integration enables the model to learn both appearance-based and motion-based patterns, making it well-suited for complex video-based activity classification tasks.

3.2.1 Spatial feature extraction via Customized Inception-V3 Network

The proposed framework utilizes a customized inception-V3 architecture, specifically tailored to enhance spatial feature extraction for human activity recognition tasks. Modifications to the standard Inception modules include the strategic integration of pooling operations within individual branches

to improve feature diversity and hierarchical abstraction. In the first Inception block, a Max-pooling (3×3) operation is added alongside Convolutional branches to capture dominant spatial activations early in the network. The second block is enhanced with both Average-pooling (3×3) after three Convolutional layers and Max-pooling (3×3) after two Convolutional layers, promoting multi-scale feature fusion. The third and fourth blocks continue this pattern with the pooling operations placed at various depths within the branches to extract increasingly abstract representations. The network concatenates all the blocks and finally passes through an 8×8 Final Global Average Pooling layer, reducing the feature map to a compact $1 \times 1 \times 1024$ tensor. This refined design facilitates the generation of a robust 1024-dimensional feature vector that encodes discriminative spatial information crucial for downstream temporal modeling.

$$y_{i,j} = \sum_{u=1}^r \sum_{v=1}^c z_{i+u-1,j+v-1} \cdot k_{u,v} \quad (2)$$

$$y_{i,j}^{\text{avg}} = \frac{1}{t^2} \sum_{u=1}^t \sum_{v=1}^t z_{i+u-1,j+v-1} \quad (3)$$

$$y_{i,j}^{\text{max}} = \max_{u=1,\dots,t; v=1,\dots,t} z_{i+u-1,j+v-1} \quad (4)$$

$$Y_{i,j,:} = [y_{i,j,:}^{(1)}, y_{i,j,:}^{(2)}, \dots, y_{i,j,:}^{(N)}] \quad \text{with } D = \sum_{n=1}^N d_n \quad (5)$$

$$h_k = f \left(\sum_p v_p W_{p,k}^{(1)} + b_k^{(1)} \right) \quad (6)$$

$$v_p = \text{Flatten}(Y) \quad (7)$$

$$f_n = f \left(\sum_k h_k W_{k,n}^{(2)} + b_n^{(2)} \right) \quad (8)$$

$$\mathbf{f} = [f_1, f_2, \dots, f_{1024}]^\top \quad (9)$$

The customized inception-V3 architecture processes spatial features through a series of convolution and pooling operations. Initially, spatial features are extracted using a standard convolution operation, as defined in Equation 2, where the input feature map z is convolved with a kernel k of size $r \times c$ to produce the output $y_{i,j}$. To reduce the spatial dimensions while preserving contextual information, average pooling is applied (Equation 3) by computing the mean value over a $t \times t$ local region. Average pooling further makes stronger activations by smoothing feature maps to reduce noise from background or lighting variations, preventing overfitting by reducing sensitivity to irrelevant details, and stabilizing temporal consistency across frames, thereby retaining subtle movement cues such as those in “walking.”

In parallel, max pooling is performed (Equation 4) to capture the most salient features within the same region. It learns region-specific variations and their characteristic boundaries [30, 31]. Max-pooling selects the strongest activation functions within the pooling region, emphasizing dominant, discriminative features by capturing key motion cues such as joint positions or sharp limb movements. It increases translation invariance to small spatial shifts and reduces irrelevant background by discarding weaker activations [32]. Additionally, it speeds up computation by shrinking feature maps without losing essential details, ensuring that critical actions like the leg motion in a “soccer kick” remain prominent. The outputs from multiple parallel branches (such as different filter sizes or pooling strategies) are then concatenated depth-wise to form a unified feature map Y , as shown in Equation 5, where the total number of channels D is the sum of the individual branch depths. This concatenated feature map is flattened into a 1D vector v (Equation 7) to prepare it for fully connected layers. The first fully connected layer transforms v into a higher-level abstract representation h_k using learned weights and a non-linear activation function f , as illustrated in Equation 6. This is followed by a second dense layer (Equation 8), which refines these features into final activations f_n . The complete

1024-dimensional feature vector \mathbf{f} , shown in Equation 9, serves as the final spatial representation extracted from the image and is subsequently passed to the temporal modeling module, such as an AA-LSTM network.

3.2.2 Spatio-Temporal Representation via Attention-Augmented LSTM

Following the extraction of spatial features from each frame using the customized InceptionV3 model, sequences of 20 consecutive 1024-dimensional vectors, representing one video segment, are used to train an AA-LSTM network. The AA-LSTM is designed with 128 hidden units and is trained to model temporal dependencies across the sequential spatial features, learning dynamic transitions and contextual patterns associated with various human activities. After training, the AA-LSTM is detached from its classification objective and repurposed as a temporal feature extractor. For each input sequence of shape $(20, 1024)$, the trained AA-LSTM processes the temporal structure and outputs a 128-dimensional feature vector corresponding to its final hidden state. This vector serves as a compact spatial-temporal representation, enriched with both appearance-based and motion-based information, and is used in subsequent stages such as feature fusion or classification.

$$\mathbf{F} = [\mathbf{F}_1, \mathbf{F}_2, \dots, \mathbf{F}_T], \quad \mathbf{F}_t \in \mathbb{R}^{1024} \quad (10)$$

$$[\mathbf{i}_t, \mathbf{f}_t, \mathbf{o}_t, \tilde{\mathbf{c}}_t] = \sigma(\mathbf{W} \cdot [\mathbf{h}_{t-1}, \mathbf{F}_t] + \mathbf{b}) \quad (11)$$

$$\mathbf{c}_t = \mathbf{f}_t \odot \mathbf{c}_{t-1} + \mathbf{i}_t \odot \tilde{\mathbf{c}}_t \quad (12)$$

$$\mathbf{h}_t = \mathbf{o}_t \odot \tanh(\mathbf{c}_t) \quad (13)$$

$$e_t = \mathbf{v}^\top \tanh(\mathbf{W}_a \cdot \mathbf{h}_t + \mathbf{b}_a) \quad (14)$$

$$\alpha_t = \frac{\exp(e_t)}{\sum_{k=1}^T \exp(e_k)} \quad (15)$$

$$\mathbf{T} = \sum_{t=1}^T \alpha_t \cdot \mathbf{h}_t \in \mathbb{R}^{128} \quad (16)$$

To effectively model both spatial and temporal dependencies within a video, frame-level spatial features $\mathbf{F}_t \in \mathbb{R}^{1024}$ are first extracted for each of the T frames, forming a sequential input $\mathbf{F} = [\mathbf{F}_1, \mathbf{F}_2, \dots, \mathbf{F}_T]$ as defined in Equation 10. These features are then fed into a customized AA-LSTM network, which learns temporal transitions across time steps. At each time step t , the AA-LSTM computes the input gate \mathbf{i}_t , forget gate \mathbf{f}_t , output gate \mathbf{o}_t , and the candidate cell state $\tilde{\mathbf{c}}_t$ based on the previous hidden state \mathbf{h}_{t-1} and the current input \mathbf{F}_t , as shown in Equation 11. The cell state \mathbf{c}_t is updated using Equation 12, and the corresponding hidden state \mathbf{h}_t is computed according to Equation 13.

To enable the model to focus selectively on important time steps, an attention mechanism is integrated. Alignment scores e_t are calculated using a feedforward layer with a learnable attention weight vector \mathbf{v} , as described in Equation 14. These scores are then normalized using the softmax function to obtain attention weights α_t (Equation 23), which reflect the importance of each hidden state \mathbf{h}_t in the overall sequence context. The final temporal representation $\mathbf{T} \in \mathbb{R}^{128}$ is obtained as a weighted sum of the hidden states (Equation 16), serving as a compact, attention-enhanced encoding of the video sequence.

3.3 Features Selection

FS plays a critical role in the development of efficient and robust machine learning models, particularly in high-dimensional datasets such as those used in video-based HAR. By identifying and retaining only the most relevant and informative features, FS helps reduce model complexity, minimize overfitting, improve generalization, and significantly lower inference time. It also enhances the interpretability of the model by focusing on features that contribute most to the classification task. The FS process typically involves evaluating the relevance, redundancy, and contribution of each feature using statistical measures, model-based techniques, or optimization algorithms. In this study, a systematic FS approach was applied, which began with extracting a comprehensive set of spatial and temporal

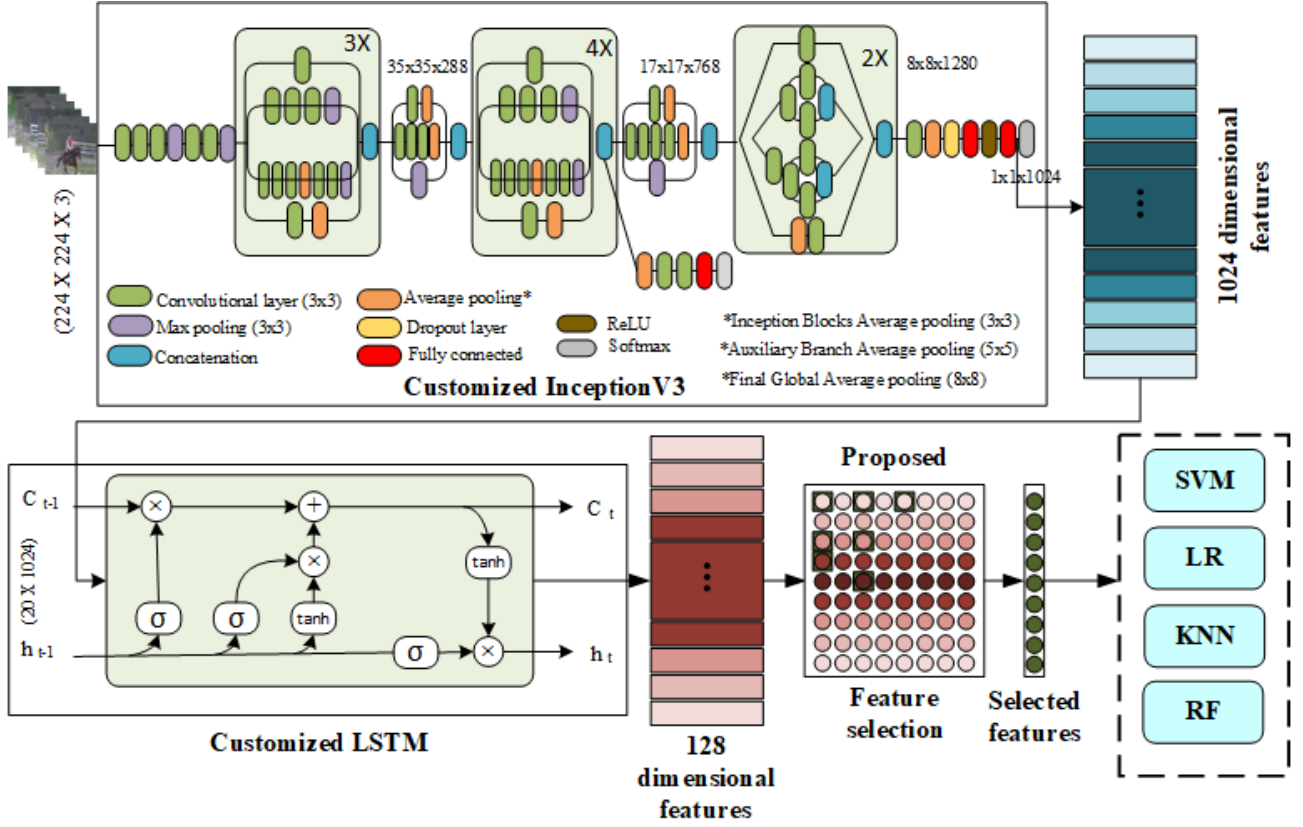


Figure 3. Detailed overview of Proposed Framework

features. These features were then evaluated using methods such as PCA [33], RFE [34], and a proposed ensemble-based fitness function to identify the most discriminative subset. The selected features were subsequently used to train lightweight classifiers, ensuring both high accuracy and computational efficiency.

3.3.1 Dynamic Fitness Sharing for Feature Selection

During the process of FS, the main population is divided into sub-populations to prevent an excessive increase in individuals within a specific high point. This strategy results in individuals gradually shifting from one peak to another peak, as their numbers rise. The method achieves this by lowering the fitness score of similar individuals as their population grows. It is assumed that similar individuals belong to the same group and occupy the same niche. A similarity measure and a threshold (niche radius) are established in the search space to determine when individuals are considered similar and part of the same niche. Studies have shown that with a sufficiently large population size and appropriately set niche radius, this approach can create as many species as there are peaks in the fitness landscape, effectively covering all niches [35].

To counteract the selection pressure issue in Fitness Sharing methods, the fitness scores of individuals within a particular peak or niche are modified. This adjustment is based on the density of similar individuals in the vicinity, operating under the assumption that individuals with similar traits belong to the same niche. The similarity between two individuals is determined using a metric, which can be applied in either the genotypic or phenotypic space. A threshold value is then used to define the maximum permissible distance for individuals to be considered similar and part of the same niche [35]. The modified DFS is discussed in the coming section in detail.

3.3.2 Proposed Novel Ensemble Adaptive Dynamic Fitness Sharing with Attention Mechanism (ADFSA)

An ensemble fitness function is proposed for feature set optimization in HAR. The proposed technique integrates multiple criteria, classification accuracy, feature redundancy, uniqueness, and complexity into a unified optimization framework using a dynamically adaptive weighting strategy. This ensemble fitness function is designed to guide the give GA-based search process to identify an optimal subset of features that are both discriminative and compact.

The ADFSA technique involves three stages:

1. **Adaptive niching Based on Feature Redundancy:** Creating 'niches' dynamically will introduce redundancy in characteristics that cannot be eliminated only by considering standard distance metrics such as the Hammer distance. In the final selection, penalizing the feature subsets that have too many similar features leads to model performance degradation and overfitting. A feature subset having high redundancy can be computed by correlation and mutual information between features, and applying a redundancy penalty.
2. **Uniqueness-Based Exploration:** Those prioritized features that were not explored in the previous generations are assigned a uniqueness score. The idea is to penalize common subsets and reward unique ones that have not been sampled frequently. Keep track of the selected features across the generations and reward with the subset features that deviate from historical selections.
3. **Hybrid Objective Optimization:** In DFS, typically focuses on optimizing accuracy (or another performance metric), introducing uniqueness will combine accuracy with model interoperability or computation cost as an addition. For example, rewarding features that lead to simpler models (fewer features, lower computation costs) while preserving accuracy leads to a hybrid fitness function. The hybrid fitness function combines accuracy, redundancy, and model complexity. The overall flow of the proposed FS is given in Figure 4

3.3.3 Mathematical Interpretation of our Proposed ADFSA Technique

The proposed technique combines multiple factors, accuracy, redundancy, uniqueness-boost, and complexity into a dynamic FS framework. The following is the mathematical representation of the ADFSA scheme incorporated in the proposed framework.

1. **Fitness Function:** The fitness function evaluates the feature subset (as a binary vector representation) and aims for high accuracy optimization by penalizing complexity and redundancy. Mathematically, it can be represented as:

$$\mathcal{F}(S) = \alpha(g) \cdot f_{acc}(S) - \beta(g) \cdot f_{red}(S) + \gamma(g) \cdot f_{uni}(S) - \delta(g) \cdot f_{comp}(S) \quad (17)$$

where $\alpha(g)$, $\beta(g)$, $\gamma(g)$, and $\delta(g)$ denote the generation-dependent weights assigned to the corresponding components of the fitness function, these weights dynamically control the influence of classification accuracy, redundancy penalty, uniqueness-boost, and complexity penalty, respectively. Typically, the weights satisfy the constraint $\alpha(g) + \beta(g) + \gamma(g) + \delta(g) = 1$, and are adjusted empirically based on the optimization stage. The binary vector S represents the selected feature subset, where a value of 1 indicates a selected feature and 0 indicates otherwise. The terms f_{acc} , f_{red} , f_{uni} , and f_{comp} correspond to the classification accuracy, redundancy measure, uniqueness score, and complexity measure, respectively, as defined in Equations (2) through (5).

2. **Accuracy Term:** This term measures the ability of the performance of a selected feature subset in terms of classification, often calculated by cross-validation on a training set as follows:

$$f_{acc}(S) = \frac{1}{k} \sum_{i=1}^k Accuracy(S_i) \quad (18)$$

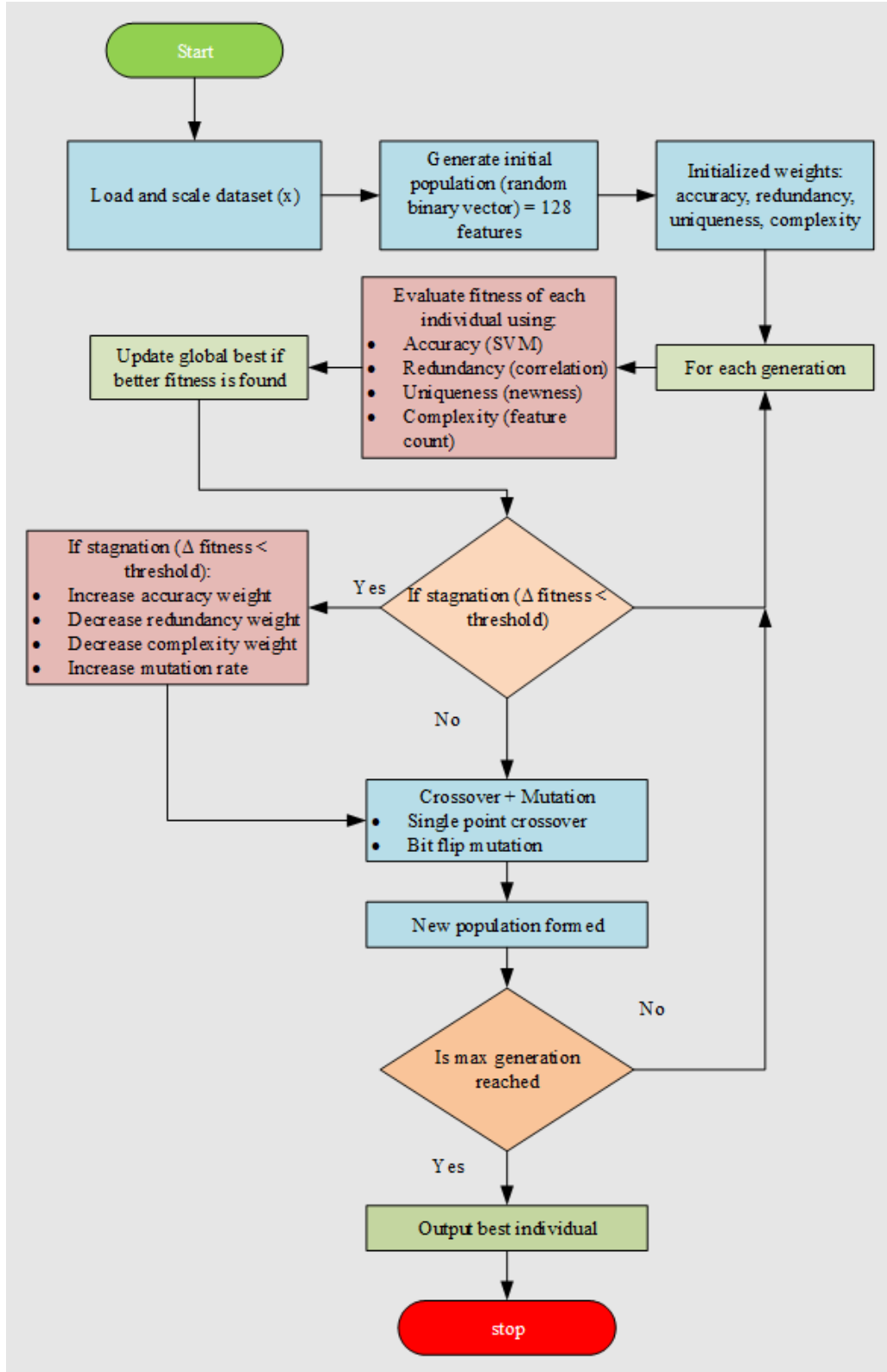


Figure 4. Flow of GA incorporated Proposed Ensembled ADFSA

where S_i represents the selected subset of features at the i -th cross-validation fold and K is the cross-validation fold number.

3. **Redundancy Penalty:** The redundancy score $f_{\text{red}}(S)$ is used to quantify the degree of correlation among the selected features in the subset S . It is computed based on the Pearson correlation coefficient r_{ij} between the i -th and j -th features. If the absolute correlation $|r_{ij}|$ exceeds a pre-defined threshold t (e.g., 0.7), the corresponding feature pair is considered highly redundant. This is captured using an indicator function $\mathbb{I}(|r_{ij}| > t)$, which returns 1 when the condition is true and 0 otherwise. The final redundancy score is normalized over all unique feature pairs and is given by:

$$f_{\text{red}}(S) = \frac{1}{n(n-1)} \sum_{i=1}^{n-1} \sum_{j=i+1}^n \mathbb{I}(|r_{ij}| > t) \quad (19)$$

A higher value of $f_{\text{red}}(S)$ indicates more redundancy among selected features, which is penalized in the fitness evaluation to encourage diversity and minimize overlap among feature contributions.

4. **Uniqueness-Boost:** To encourage exploration and maintain population diversity, a uniqueness reward is introduced. This reward is granted to feature subsets that have not been encountered in prior generations. It is computed as:

$$f_{\text{uni}}(S) = \mathbb{I}\{S \notin \mathcal{H}\} \quad (20)$$

where \mathcal{H} denotes the set of previously evaluated feature subsets (i.e., the search history), and $\mathbb{I}\{S \notin \mathcal{H}\}$ is an indicator function that returns 1 if the subset S is novel (not present in history), and 0 otherwise. This mechanism rewards diversity by promoting unseen solutions, thus helping to avoid premature convergence of the algorithm.

5. **Complexity Penalty:** This component discourages the selection of excessively large feature subsets, promoting model simplicity and reducing overfitting. It is calculated as:

$$f_{\text{comp}}(S) = \frac{|S|}{n} \quad (21)$$

where $|S|$ represents the number of selected features in subset S (i.e., the number of 1's in the binary selection vector), and n denotes the total number of available features. A higher value of f_{comp} indicates a more complex subset, which is penalized in the fitness function to favor parsimonious models.

To improve convergence and enhance search efficiency, the weights of the ensemble fitness function are dynamically adapted throughout the evolutionary process. The goal is to favor exploration (diversity and redundancy control) in early generations and gradually shift focus toward exploitation (accuracy and compactness) in later generations.

Let G be the total number of generations and $g \in [1, G]$ be the current generation.

Define the normalized progress as:

$$p = \frac{g}{G} \quad (22)$$

Then the weights are updated as follows:

$$\alpha(g) = 0.4 + 0.6 \cdot p \quad (\text{from } 0.4 \text{ to } 1.0) \quad (23)$$

$$\beta(g) = 0.3 - 0.2 \cdot p \quad (\text{from } 0.3 \text{ to } 0.1) \quad (24)$$

$$\gamma(g) = 0.3 - 0.2 \cdot p \quad (\text{from } 0.3 \text{ to } 0.1) \quad (25)$$

$$\delta(g) = 0.2 + 0.1 \cdot p \quad (\text{from } 0.2 \text{ to } 0.3) \quad (26)$$

In the proposed fitness function, the dynamic behavior of the evolutionary algorithm is controlled through four generation-dependent weights: $\alpha(g)$, $\beta(g)$, $\gamma(g)$, and $\delta(g)$. These weights adapt over time according to the normalized generation progress p , defined in Equation (22), where g is the current generation and G is the total number of generations.

The weight $\alpha(g)$ in Equation (23) increases linearly from 0.4 to 1.0 as p grows, placing greater emphasis on the accuracy component of the fitness function in later generations. This encourages exploitation once the algorithm has sufficiently explored the search space. Conversely, both $\beta(g)$ and $\gamma(g)$, as shown in Equations (24) and (25), decrease linearly from 0.3 to 0.1, reducing the influence of redundancy and novelty as evolution progresses. This shift reflects the reduced need for diversity and exploration in later stages. Lastly, $\delta(g)$ in Equation (26) increases slightly from 0.2 to 0.3 to mildly penalize overly complex feature subsets, promoting compact representations toward the end of the search.

This adaptive scheme ensures a smooth transition from exploration to exploitation during FS, leading to more optimal and generalizable feature subsets.

Algorithm 1 Evolutionary FS with Dynamic Adjustment

```

Set previous_best_fitness  $\leftarrow$  0
Set generation  $\leftarrow$  0
while generation < n_generations do
  if generation > 5 AND  $\max(\text{fitness\_scores}) - \text{previous\_best\_fitness} < 0.001$  then
    accuracy_weight  $\leftarrow$   $\min(\text{accuracy\_weight} + 0.05, 1.0)$ 
    redundancy_weight  $\leftarrow$   $\max(\text{redundancy\_weight} - 0.05, 0.1)$ 
    mutation_rate  $\leftarrow$   $\min(\text{mutation\_rate} + 0.01, 0.2)$ 
  end if
  Initialize fitness_scores  $\leftarrow$  []
  for each individual in population do
    fitness  $\leftarrow$  evaluate_individual(individual,  $x, y, w$ ) {Fitness function is applied here.}
    Append fitness to fitness_scores
  end for
  Sort population based on fitness_scores {Fitness scores determine sorting.}
  Select top half of population
  Initialize new_population  $\leftarrow$  []
  while  $\text{length}(\text{new\_population}) \neq \text{population\_size}$  do
    Randomly select two parents: parent1, parent2 from population
    crossover_point  $\leftarrow$  random integer between 1 and  $n\_features - 1$ 
    child1  $\leftarrow$  combine parent1 and parent2 at crossover_point
    child2  $\leftarrow$  combine parent2 and parent1 at crossover_point
    for each child in [child1, child2] do
      if random probability  $\leq$  mutation_rate then
        mutation_point  $\leftarrow$  random integer between 0 and  $n\_features - 1$ 
        Flip the value of child[mutation_point]
      end if
    end for
    Append child1 and child2 to new_population
  end while
  Set population  $\leftarrow$  new_population
  Set previous_best_fitness  $\leftarrow$   $\max(\text{fitness\_scores})$  {Updating based on fitness values.}
  Print "Generation ", generation, " complete, top fitness: ", previous_best_fitness
  Increment generation  $\leftarrow$  generation + 1
end while

```

3.3.4 Key Advantages of the Proposed Framework

The proposed framework introduces a comprehensive and adaptive FS technique that integrates four fundamental aspects, *accuracy*, *redundancy*, *uniqueness*, and *complexity* into a unified fitness function. This multi-objective formulation ensures a balanced trade-off between classification performance and model simplicity. One of the key innovations lies in the dynamic adjustment of the weights associated with each fitness component during the evolutionary process. This adaptive mechanism fosters exploration in the initial generations and shifts towards exploitation in later stages, which enhances convergence and helps avoid premature stagnation in local optima. Additionally, the method incorpo-

rates a redundancy penalty based on mutual information, effectively minimizing the selection of highly correlated features and ensuring that only the most informative attributes are retained. To further improve population diversity, a uniqueness term is introduced that rewards diverse feature subsets across generations, increasing the likelihood of identifying globally optimal solutions. The inclusion of a complexity component drives the selection of smaller, more efficient feature sets, thereby reducing the computational cost and facilitating faster model inference, an essential requirement for real-time and embedded HAR systems. Empirical evaluations demonstrate that the proposed technique outperforms traditional FS techniques such as PCA and RFE in terms of classification accuracy, even with fewer selected features. Moreover, the approach is classifier-agnostic and compatible with a variety of learning algorithms, including SVM, KNN, Random Forest (RF), and Logistic Regression (LogReg). Its scalability makes it particularly suitable for handling high-dimensional feature vectors derived from deep learning models, addressing the limitations of conventional methods related to scalability and interpretability. Overall, the proposed ensemble-based, dynamically adaptive, and diversity-aware technique presents a novel and effective solution for FS in HAR and other pattern recognition domains.

In our proposed technique, redundancy and uniqueness-boost mechanisms ensure that the algorithm does not converge too early on a suboptimal feature subset. Furthermore, the inclusion of model complexity into the fitness function will produce simpler models, which are more computationally efficient and easier to interpret. Incorporating flexibility across different types of FS tasks, and penalty terms having adaptive natures, allows fine-tuning based on the specific problem or dataset.

3.4 Classification

To assess the effectiveness of the proposed FS technique, we perform a comparative evaluation against two widely used techniques: PCA and RFE. PCA is a linear dimensionality reduction approach that transforms the feature space into orthogonal components capturing the maximum variance. RFE, on the other hand, iteratively removes the least important features based on model weights, gradually selecting the most significant subset.

Our proposed technique employs a custom-designed fitness function that adaptively balances classification accuracy f_{acc} , feature redundancy f_{red} , uniqueness f_{uni} , and complexity f_{comp} . The dynamic weighting mechanism evolves over generations, initially favoring diversity and redundancy control, and later shifting focus toward accuracy and compactness.

To evaluate classification performance and testing efficiency, the optimized features obtained from each selection method are fed into a set of lightweight machine learning classifiers, including SVM, RF, KNN, and LogReg. SVM is chosen for its strong generalization capability in high-dimensional spaces. RF offers robustness to overfitting and effectively handles noisy or complex data. k-NN serves as a non-parametric baseline suitable for low-dimensional feature spaces, while LR provides a fast, interpretable linear model as a benchmark.

Let the optimized feature vector selected by the GA be denoted as:

$$\mathbf{f}^* = [f_1^*, f_2^*, \dots, f_d^*]^\top \in \mathbb{R}^d \quad (27)$$

$$\hat{Y}_{\text{SVM}} = \text{sign}(\mathbf{w}^\top \mathbf{f}^* + b) \quad (28)$$

$$\hat{Y}_{\text{RF}} = \text{mode}(\{h_t(\mathbf{f}^*)\}_{t=1}^T) \quad (29)$$

$$\hat{Y}_{\text{kNN}} = \text{mode}(\{y_i : \mathbf{f}_i \in \mathcal{N}_k(\mathbf{f}^*)\}) \quad (30)$$

$$\hat{Y}_{\text{LR}} = \begin{cases} 1, & \text{if } \sigma(\mathbf{w}^\top \mathbf{f}^* + b) \geq 0.5 \\ 0, & \text{otherwise} \end{cases} \quad (31)$$

The optimized feature vector \mathbf{f}^* , generated through the proposed GA-based FS technique, is evaluated using multiple lightweight machine learning classifiers to assess its classification capability and generalizability. The SVM, as formulated in Equation 28, determines the class label by computing the sign of a weighted linear combination of features and bias, effectively creating a maximum-margin decision boundary. The RF classifier, shown in Equation 29, aggregates predictions from an ensemble

of T decision trees and outputs the majority-voted label, thereby reducing variance and enhancing robustness. The k-Nearest Neighbors (k-NN) approach, expressed in Equation 30, relies on the most frequent class among the k closest samples in the feature space, making it highly adaptive to local patterns in the data. LogReg, represented in Equation 31, calculates the sigmoid-activated probability and assigns the class label based on a threshold decision rule. Together, these classifiers provide a diverse set of perspectives to validate the quality of the selected features. To further benchmark the effectiveness of the proposed FS technique, classical techniques like PCA and RFE are also applied under identical evaluation settings. All models are evaluated in terms of both classification accuracy and inference time to validate the practical efficiency of the selected features.

4 Experimental Setup

The experimental setup of this research is structured into four main components. First, the dataset is introduced, highlighting its composition and class distribution. Second, a two-phase framework is applied, where spatio-temporal features are extracted using a customized deep learning architecture and then refined through the proposed feature selection technique. Third, the hardware and software environment is outlined to specify the implementation platform and computational resources used. Together, these components provide a clear foundation for evaluating the effectiveness and efficiency of the proposed framework.

4.1 Dataset

The YouTube Action Dataset [11] is a widely used benchmark in human activity recognition, consisting of diverse videos collected from YouTube that capture real-world human actions in varied contexts and environments. It covers multiple action categories such as walking, running, biking, and hand-waving, among others, making it a challenging testbed for evaluating recognition algorithms. In this research, the dataset was divided into training and testing sets using an 80/20 split to ensure balanced evaluation of the proposed framework.

What sets this dataset apart is its variability in camera angles, background clutter, lighting conditions, and motion dynamics, which better reflect real-world scenarios compared to more controlled datasets. Each video sequence is typically labeled with a single dominant activity, and many clips, as showing in Figure 5, contain temporal and spatial variations that test the robustness of recognition models. Due to its complexity and diversity, the YouTube Action Dataset has become a standard benchmark for assessing the effectiveness of deep learning architectures, spatiotemporal modeling techniques, and feature extraction frameworks in video-based activity recognition. The detailed configuration of the dataset is outlined in Table 2.

4.2 Two-Phase Feature Extraction and Selection Framework

Overall the research was implemented into two different phases. In the first phase, spatio-temporal features were extracted using a customized Inception-V3 and AA-LSTM network, and in the second phase, the extracted features were passed through the proposed ADFSA FS technique to obtain compact and robust features without affecting the performance of the underlying classifier.

4.2.1 Spatial Feature Extraction Phase

This work employs a deep CNN architecture to extract discriminative features from video frames. Extensive experiments were carried out by training several deep CNN models, as summarized in Table 3. Among the evaluated architectures, InceptionV3 consistently outperformed the others, demonstrating good recognition accuracy. Training of selected networks and the overall proposed framework is presented in Figure 6. Consequently, it was selected and customized for the HAR task, capturing diverse and robust features region and edge, leading to enhanced performance. The training and loss curves of the optimized model are illustrated in Figures 7a and 7b, respectively.



Figure 5. YouTube Action Dataset.

Table 2. Configuration of the UCF-YouTube (UCF11) Dataset

Attribute	Details
Full Name	UCF YouTube Action Dataset (UCF11)
Source	YouTube videos
Total Action Classes	11
Action Classes	Basketball Shooting, Biking, Diving, Golf Swing, Horse Riding, Soccer Juggling, Swinging, Tennis Swing, Trampoline Jumping, Volleyball Spiking, Walking with a Dog
Total Video Clips	1,600
Clips per Class	Approximately 145 (varies slightly)
Resolution	320×240 (typical, but varies)
Frame Rate	29.97 fps (varies)
Video Format	.avi
Total Groups	25 per class (each group has different people/backgrounds/camera motions)
Group-wise Split	Leave-one-group-out cross-validation commonly used
Duration per Clip	Approximately 4–10 seconds
Labels	Provided via folder structure (one folder per class)
Modality	RGB (no audio/depth/skeleton)
Tasks Supported	Action Recognition, Temporal Segmentation
Preprocessing Required	Frame extraction, resizing, normalization
Common Benchmarks	Accuracy, Precision, Recall, F1-score
Download URL	http://cvcv.ucf.edu/data/UCF_YouTube_Action.php

In the feature extraction stage, each input video is decomposed into a sequence of frames at a fixed sampling rate to capture meaningful visual cues. These frames are resized and normalized before being

passed through the customized InceptionV3 network, which is employed as a deep feature extractor. Specifically, the frames are processed up to the final global average pooling layer, producing a 1024-dimensional feature vector per frame. These features encode high-level spatial representations of the visual content, capturing semantic attributes such as shapes, textures, and object structures. The extracted frame-wise features are then stored sequentially to preserve their temporal order for subsequent processing stages.

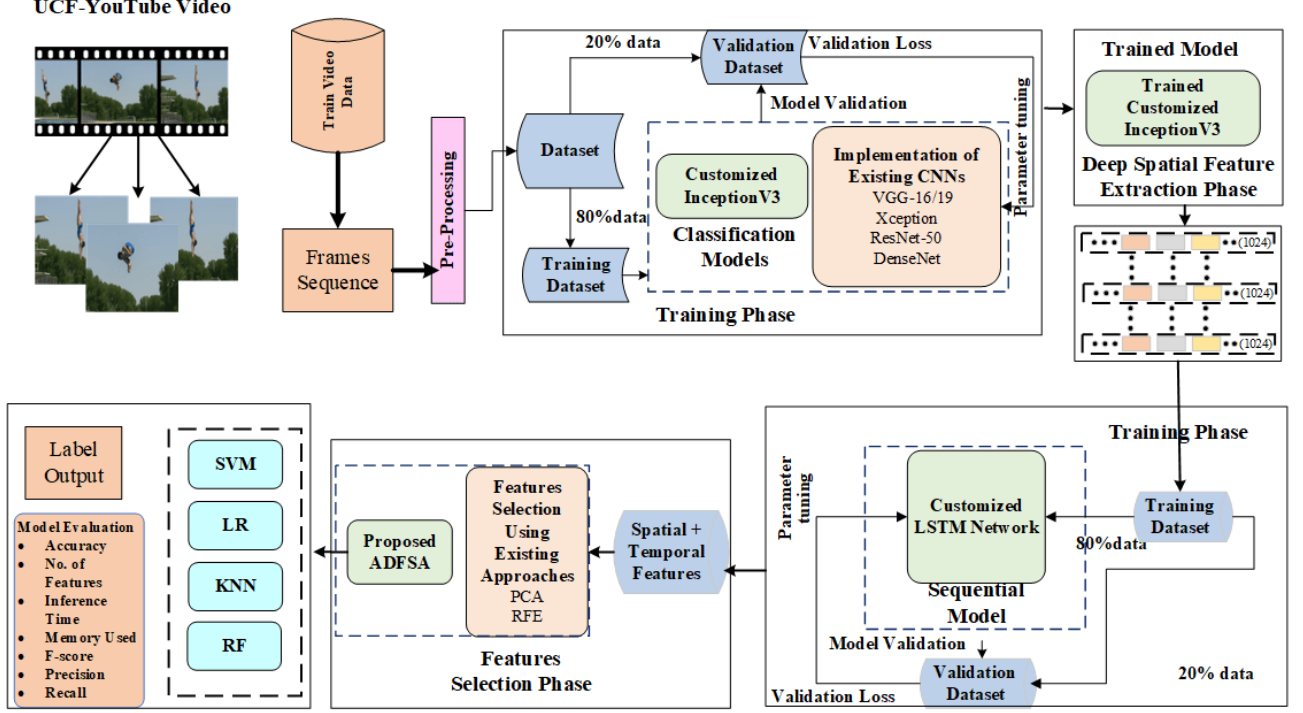


Figure 6. Experimental setup of Proposed Framework

4.2.2 Temporal Feature Learning using AA-LSTM

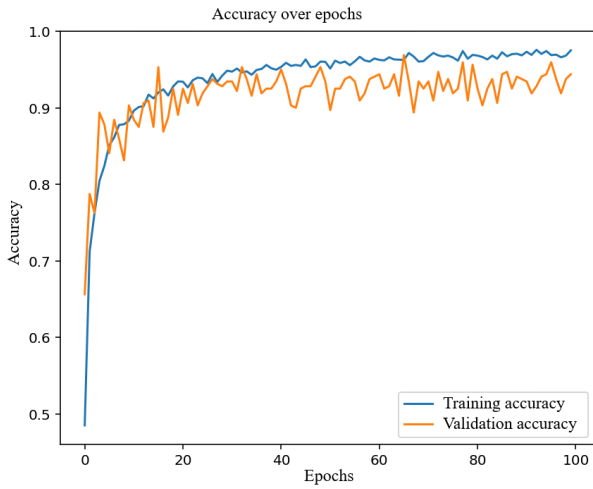
To capture the temporal dynamics present across consecutive video frames, an AA-LSTM network is employed. Features of 20 frames extracted from customized Inception-V3 in a sequential manner are fed into the AA-LSTM, learning long-range dependencies between consecutive individual frames, retaining historical context over time. In this setup, the AA-LSTM network consists of 128 memory units and is trained using the frame-wise feature vectors in sequence. This enables the model to understand motion patterns, temporal transitions, and dependencies between frames that are critical for activity recognition. After training, the AA-LSTM outputs a feature representation that integrates both spatial information (from InceptionV3) and temporal dependencies (learned via AA-LSTM). These fused spatio-temporal features are then used for subsequent feature optimization and classification tasks.

4.2.3 Features Selection via ADFSA

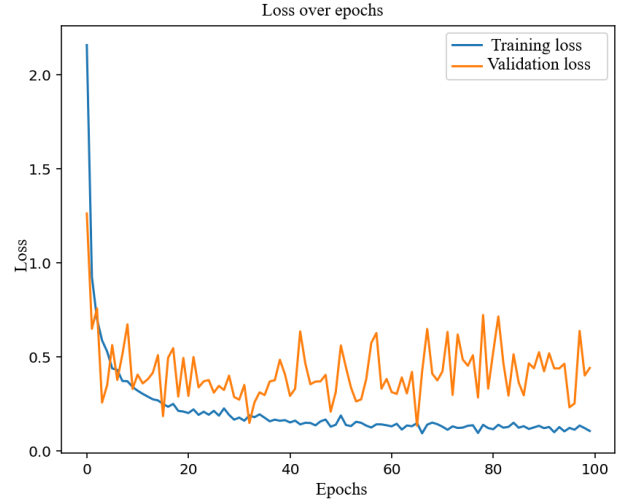
To enhance the quality of the extracted features, an optimization step was carried out using the proposed ADFSA algorithm. This method leverages a GA guided by an ensemble-based fitness function that integrates four complementary evaluation criteria. First, *classification accuracy* is assessed using stratified 5-fold cross-validation with a linear SVM, ensuring robust performance estimation. Second, a *redundancy penalty* based on mutual information is incorporated to discourage the selection of highly correlated features, promoting a more informative subset. Third, a *uniqueness component* is introduced to enhance population diversity by penalizing the recurrence of identical feature subsets across generations. Finally, a *complexity term* penalizes larger subsets, thereby encouraging compact and computationally efficient FSs. Notably, the relative weights of these components are adaptively updated throughout the evolutionary process, guided by the normalized progression of the population's fitness. This dynamic adjustment ensures a balance between exploration and exploitation, ultimately

Table 3. Different selected Deep CNN

Methods	Accuracy
Xception	94.42%
VGG-16	95.35%
VGG-19	95.63%
Resnet-50	88.34%
ResNet50-v2	98.73%
Resnet-152	81.24%
ResNet-101	78.33%
DenseNet-121	96.89%
DenseNet-169	96.90%
NasNet-Large	96.86%
Inception-V3	97.07%
Customized Inception-V3	98.15%
Customized Inception-V3 + AA-LSTM	99.32%



(a) Model Accuracy.



(b) Model Loss.

Figure 7. InceptionV3 Model Accuracy and Loss during Training.

leading to the selection of high-quality, low-redundancy feature sets well-suited for classification tasks. To assess the effectiveness of the proposed technique, two widely used FS techniques were implemented, PCA [25] and RFE [26]. The effectiveness of various selection methods was assessed using a range of classification algorithms, comprising SVM, RF, KNN, and LogReg.

4.3 Hardware and Implementation

All machine learning classifiers and FS algorithms were implemented and executed using the Spyder integrated development environment (IDE). The codebase was implemented in python 3.10, utilizing TensorFlow/Keras, Scikit-learn, openCV, and NumPy libraries. The experiments related to traditional ML models, such as SVM, RF, KNN, and LogReg, were conducted on a system equipped with an Intel Core i7 10th-generation processor and 16 GB of RAM. For the training of deep CNN, including customized InceptionV3 and AA-LSTM-based models, a high-performance computing setup was used, consisting of an HP desktop powered by an Intel Core-i9 9th-generation processor, 64 GB of RAM, and an NVIDIA GeForce RTX 2080 Ti GPU, all the configuration is given in Table 4. This dual-platform configuration was essential to accommodate both lightweight ML tasks and compute-intensive deep learning workloads effectively.

Table 4. Configuration details of the experimental setup.

Component	Details
Backbone Network	Customized inceptionV3 (pretrained)
Temporal Model	Customized AA-LSTM with 128 units
Input Size	$224 \times 224 \times 3$
Frames per Video	20
Optimizer	Adam ($\text{lr} = 1 \times 10^{-4}$)
Batch Size	32
Loss Function	Categorical Cross-Entropy
Training Epochs	100
Hardware	NVIDIA RTX 2080 Ti, 32 GB RAM

5 Results and Discussions

Extensive experiments were conducted on benchmark HAR datasets to evaluate the proposed dynamic composite fitness function for feature selection. Compared with PCA and RFE, the method achieved higher accuracy, selected fewer features, and improved inference speed. By adjusting the balance between accuracy, redundancy, uniqueness, and complexity, the fitness function guided the search toward compact yet effective feature subsets. In one case, only 7 out of 128 features were selected while still reaching a test accuracy of 99.58%, along with reduced memory use and faster execution. These results show that the method can provide accurate and efficient recognition, even in real-time or resource-limited settings.

The detailed results are presented in the following subsections. First, 2D feature space visualizations are shown to highlight the separability of the optimized features. Next, evaluation metrics and implementation settings are described. This is followed by a performance summary along with memory and training time analysis. Additional measures such as F1-score, precision, and recall are then reported to provide a broader view of classification performance. An ablation study is included to examine the contribution of each component of the fitness function. Finally, the proposed technique is compared with state-of-the-art approaches to demonstrate its overall effectiveness.

5.1 2D Features Space Visualization

Visualization shown in Figure 8a appears to show a relatively linear, diagonal clustering trend across the latent feature space. The color gradient representing "Feature Labels" is moderately well-separated, with neighboring clusters transitioning smoothly. However, there is still a significant degree of overlap between different class regions, especially in the bottom-left and center areas. This overlap may suggest that while AA-LSTM has captured some degree of class-specific information, it lacks sharp class boundary definitions, potentially due to noise or insufficient feature discrimination.

The RFE approach exhibits a more refined clustering compared to AA-LSTM as shown in Figure 8b. The class transitions (as per the color bar) are smoother, and the data points are more tightly grouped. However, there is still observable overlap at the cluster borders. RFE seems to preserve the intrinsic feature structure more effectively than AA-LSTM, indicating better dimensional reduction and selection fidelity. Nevertheless, this method may still struggle with high inter-class similarity, particularly in the mid-spectrum of the feature labels.

The 2D visualization of the reduced feature space reveals a dispersed and overlapping distribution of class labels, with a significant concentration of data points along the boundary axes as shown in Figure 9a. While certain regions, particularly the upper-left quadrant show partial grouping of higher-class labels, the overall structure lacks clear separation and compactness among different classes. The compression of points near the plot edges suggests potential information loss during dimensionality reduction, which may affect the ability to distinguish between classes effectively. This scattered layout indicates limited class discriminability, emphasizing the need for more robust feature extraction or selection techniques to preserve the underlying semantic relationships within the data.

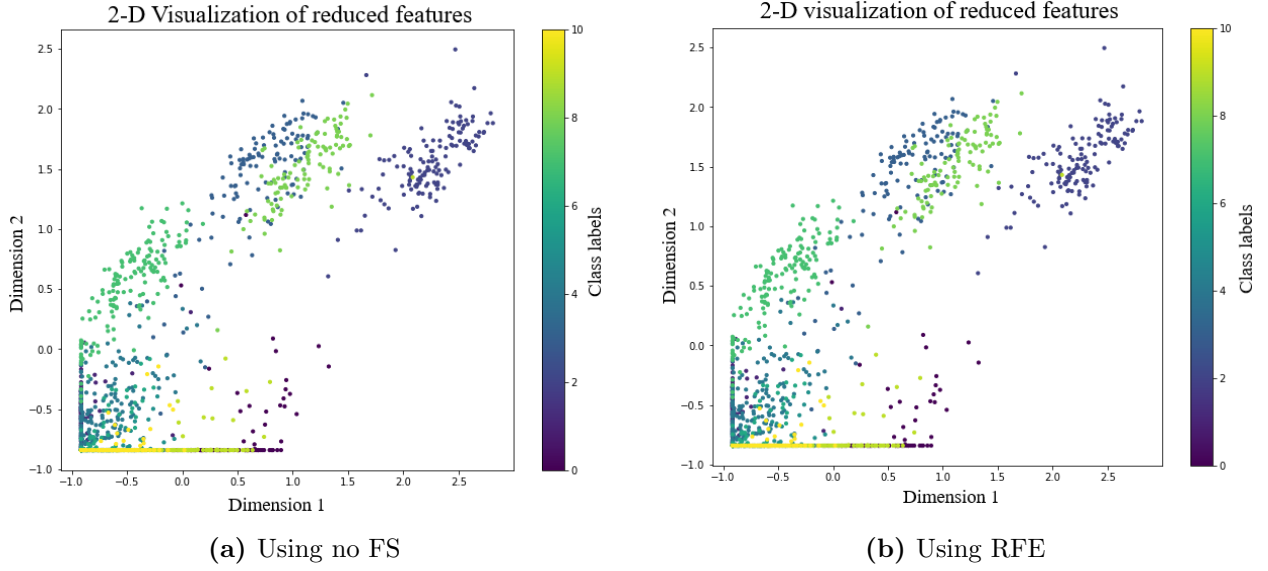


Figure 8. Feature space visualization with no FS vs RFE.

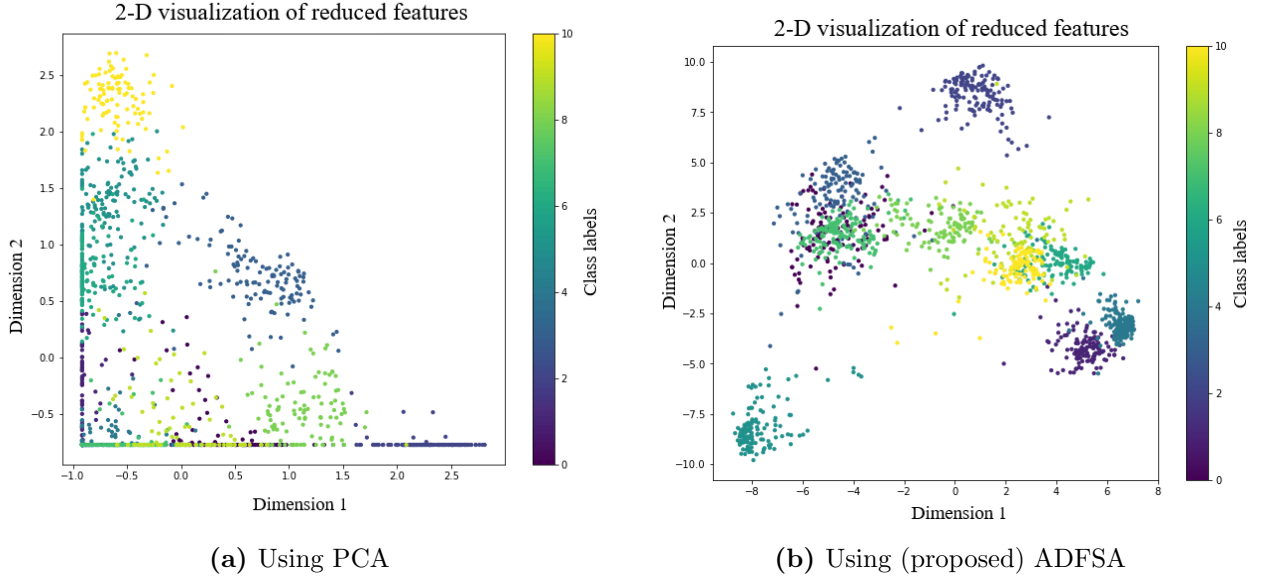


Figure 9. Feature space visualization with PCA vs Proposed ADFSFA.

The most notable contrast is seen in the visualization using the proposed ADFSFA technique shown in Figure 9b. This plot shows distinct and well-separated clusters, with a clearer demarcation among different feature label zones. The visualized feature space demonstrates improved intra-class compactness and inter-class separation, indicating superior FS and reduction capabilities. The spread of clusters in multiple directions suggests that ADFSFA captures more complex relationships within the data, which may translate to better generalization and classification performance in downstream tasks.

5.2 Evaluation Metrics

To comprehensively evaluate the performance of the proposed framework, several quantitative metrics were employed. Classification accuracy (%) was computed on the test set to assess the overall predictive capability of the model by Equation 32. In addition, the precision, recall, F1-score, were used to provide a more balanced evaluation, particularly in the presence of class imbalance by Equations 33–35. The number of selected features was recorded to reflect the dimensionality reduction achieved through the FS process. To assess computational efficiency, the average inference time (in milliseconds) was measured over five independent runs. Furthermore, memory usage (in KB) of the selected features was

analyzed to evaluate the memory footprint of the model. These metrics together offer a holistic view of the classification performance, computational efficiency, and practicality of the proposed framework.

$$\text{Accuracy} = \frac{TP}{TP + FP + FN} \quad (32)$$

$$\text{Precision} = \frac{TP}{TP + FP} \quad (33)$$

$$\text{Recall} = \frac{TP}{TP + FN} \quad (34)$$

$$\text{F1-score} = \frac{2 \times \text{Precision} \times \text{Recall}}{\text{Precision} + \text{Recall}} \quad (35)$$

5.3 Performance Summary

Table 5 presents a comparative analysis of the proposed ADFSFS technique against conventional techniques including PCA and RFE across four widely used classifiers: SVM, RF, KNN, and LogReg. The evaluation is based on three key metrics: cross-validation accuracy, number of selected features, and average inference time over five runs. The ADFSFS method consistently achieves the highest accuracy across all classifiers, reaching up to 99.65% for RF, while significantly reducing the feature set to only seven features. This demonstrates the method’s capability to retain highly discriminative features while discarding redundant or irrelevant ones. Additionally, ADFSFS achieves the lowest inference times in all cases, indicating its suitability for real-time human activity recognition applications. The combined improvements in accuracy, feature compactness, and computational efficiency clearly highlight the superiority of the proposed ensemble fitness function over traditional FS techniques.

Table 5. Performance comparison of different FS methods using various classifiers.

Classifier	Setting	CV Accuracy(%)	# Features	Avg. Inf. Time (ms)
SVM	No FS	97.35	128	1.242
	PCA	97.79	50	0.313
	RFE	97.73	50	0.468
	ADFSFS	99.58	7	0.196
RF	No FS	97.23	128	19.189
	PCA	97.45	50	13.542
	RFE	97.51	50	10.717
	ADFSFS	99.65	7	8.714
KNN	No FS	97.32	128	17.945
	PCA	97.54	50	8.033
	RFE	97.44	50	17.676
	ADFSFS	99.58	7	6.958
LogReg	No FS, No Reg	97.39	128	0.780
	PCA	97.58	50	0.966
	RFE	97.57	50	0.202
	ADFSFS	99.51	7	0.173

Table 6 presents a comparative analysis of four different FS techniques, PCA, RFE, and the proposed ADFSFS, evaluated across multiple classifiers, including SVM, RF, KNN, and LogReg. The percentage changes in cross-validation (CV) accuracy, number of selected features, and inference time are reported relative to the baseline scenario without FS (No FS). Among the FS methods, ADFSFS consistently delivers the most substantial improvement in classification accuracy, with gains ranging from +2.18% to +2.49% across all classifiers. Moreover, ADFSFS achieves the highest reduction in feature dimensionality (approximately 94.5%) and inference time (up to 84.2%), indicating its effectiveness in optimizing both performance and computational efficiency. In contrast, PCA and RFE offer moderate improvements in accuracy and feature reduction but are comparatively less impactful in reducing

inference time. Notably, PCA increases inference time for LogReg, suggesting that dimensionality reduction alone does not always guarantee runtime efficiency. These findings underscore the advantage of ADFSAs as a robust and scalable FS strategy for improving model performance while significantly reducing computational overhead.

Table 6. Percentage change (%) in CV Accuracy, Number of Features, and Inference Time compared to baseline (No FS) for each classifier.

Classifier	Setting	Δ Acc. (%)	Δ # Features (%)	Δ Inf. Time (%)
SVM	No FS	0.00	0.00	0.00
	PCA	+0.45	-60.94	-74.80
	RFE	+0.39	-60.94	-62.32
	ADFSAs (Proposed)	+2.29	-94.53	-84.22
RF	No FS	0.00	0.00	0.00
	PCA	+0.23	-60.94	-29.43
	RFE	+0.29	-60.94	-44.15
	ADFSAs (Proposed)	+2.49	-94.53	-54.59
KNN	No FS	0.00	0.00	0.00
	PCA	+0.23	-60.94	-55.24
	RFE	+0.12	-60.94	-1.50
	ADFSAs (Proposed)	+2.32	-94.53	-61.23
LogReg	No FS	0.00	0.00	0.00
	PCA	+0.20	-60.94	+23.85
	RFE	+0.18	-60.94	-74.10
	ADFSAs (Proposed)	+2.18	-94.53	-77.82

Figures 10 and 11 illustrate a comprehensive comparative evaluation of different FS methods applied to SVM and RF classifiers, respectively. The results clearly highlight the superior performance of the proposed ADFSAs technique in all metrics considered. For the SVM classifier, ADFSAs achieves the highest accuracy of 99.58%, outperforming traditional methods such as PCA and RFE, which yield 97.79% and 97.73%, respectively. Notably, ADFSAs also uses only 7 features, significantly fewer than PCA (50) and the baseline (128), demonstrating its efficiency in dimensionality reduction. Additionally, it reports the lowest inference time of 0.196 ms, indicating suitability for real-time scenarios.

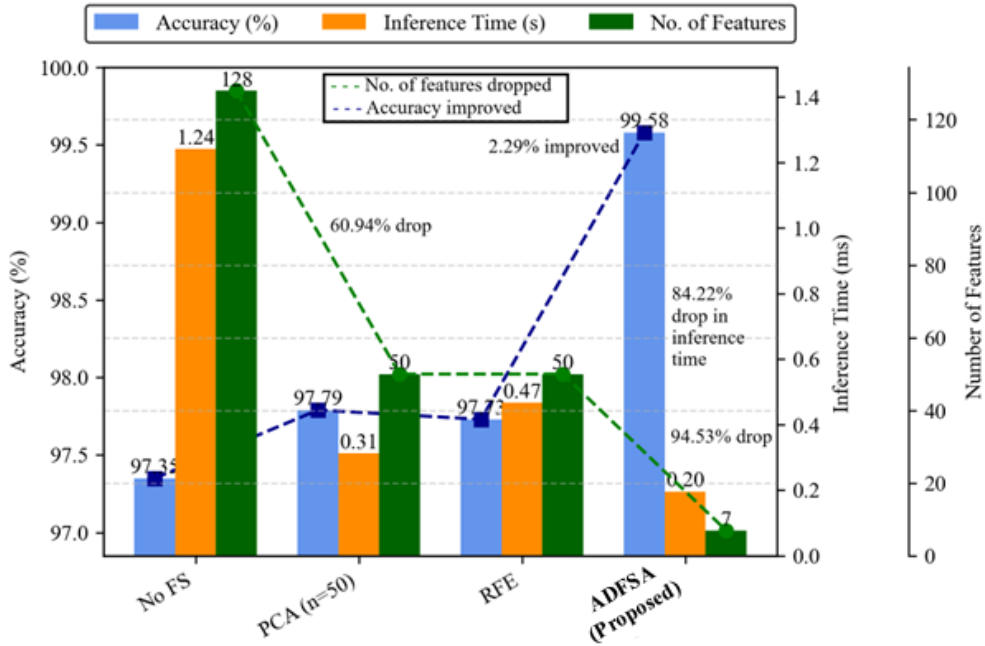


Figure 10. Comparative Analysis using SVM.

Similarly, in the case of the RF classifier (Figure 11), the proposed technique achieves the best accuracy

of 99.65%, compared to 97.45% with PCA and 97.51% with RFE. It also maintains a reduced feature set of 7 while lowering the inference time to 8.714 ms, which is significantly faster than the baseline method (19.189 ms). These results affirm that ADFSFA not only preserves or improves classification performance but also reduces computational overhead, making it highly effective for Human Activity Recognition tasks where both accuracy and real-time efficiency are crucial.

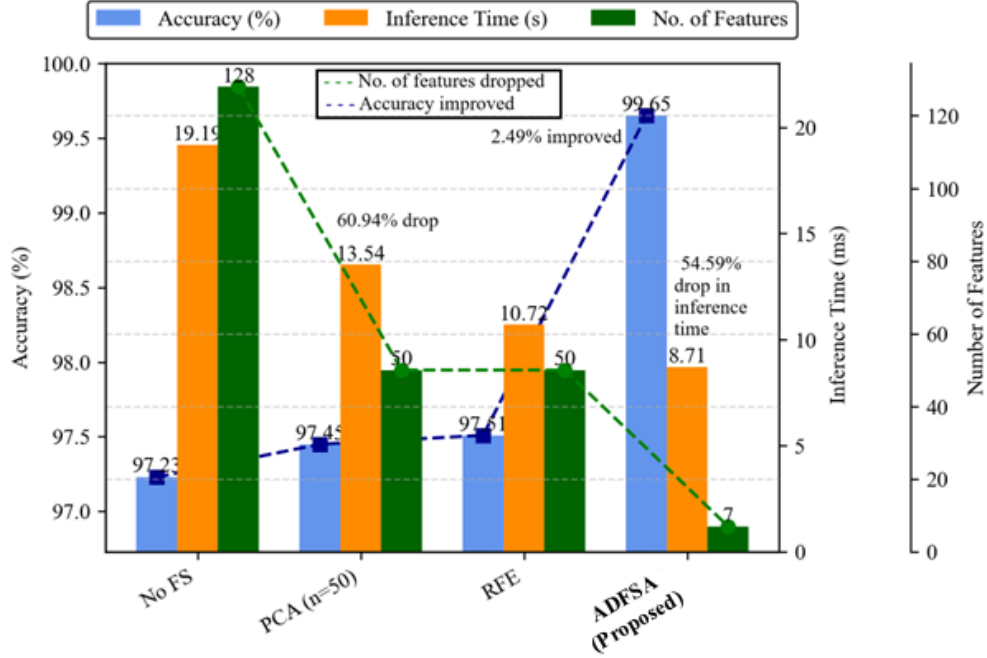


Figure 11. Comparative Analysis using RandomForest.

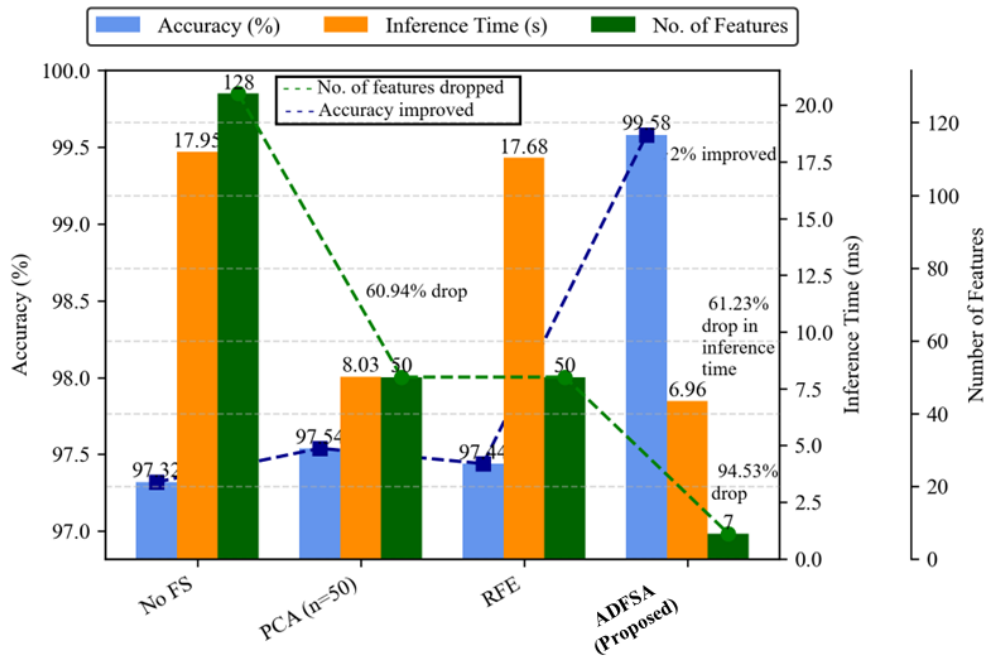


Figure 12. Comparative Analysis using KNN.

Figures 12 and 13 further validate the effectiveness of the proposed ADFSFA FS technique when applied to KNN and LogReg classifiers. For the KNN classifier (Figure 12), ADFSFA achieves the highest accuracy of 99.58%, outperforming PCA (97.54%) and RFE (97.44%). More importantly, it reduces the number of features to just 7, compared to 50 for PCA/RFE and 128 in the baseline.

Inference time also shows a significant improvement, dropping to 6.958 ms, whereas PCA and RFE report 8.033 ms and 17.676 ms, respectively. This performance reinforces the scalability of ADFSA even in non-parametric models like KNN.

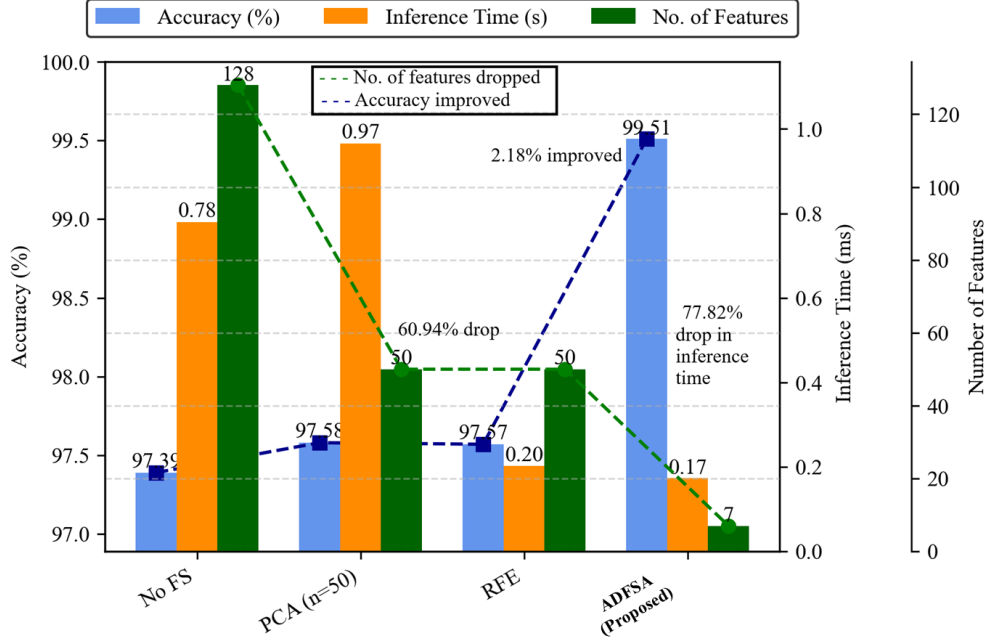


Figure 13. Comparative Analysis using LogReg.

Similarly, Figure 13 shows that in the case of LogReg, ADFSA achieves 99.51% accuracy, significantly higher than the baseline (97.39%), PCA (97.58%), and RFE (97.57%). It also demonstrates the most efficient inference time at 0.173 ms, with only 7 selected features. In contrast, PCA and RFE require 50 features each and yield higher inference times of 0.966 ms and 0.202 ms, respectively. These results highlight the strong generalization of the proposed technique in different types of classifiers while consistently reducing computational cost and improving classification performance.

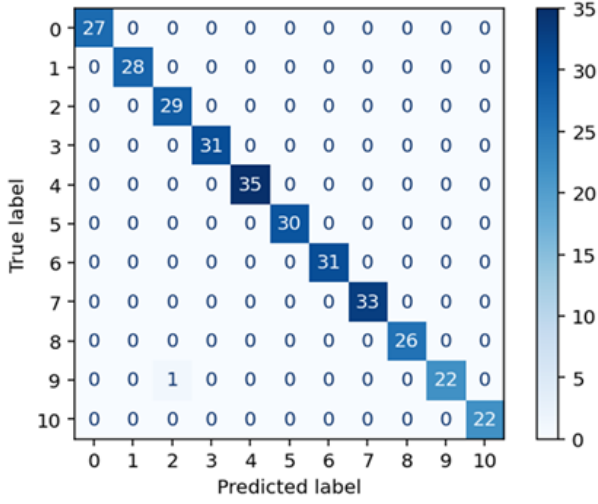
Figure 14a and Figure 14b present the confusion matrices for SVM and Random Forest classifiers, respectively. Both classifiers exhibit strong discrimination capability across the 11 activity classes. In each case, the confusion matrix demonstrates clear diagonal dominance, indicating that the majority of the test samples were correctly classified. Only a few isolated off-diagonal entries are present, suggesting minimal misclassifications between activity classes.

Figure 15a and Figure 15b illustrate the confusion matrices for the KNN and Logistic Regression classifiers. Similar to SVM and Random Forest, both classifiers achieve consistent recognition performance with strong diagonal dominance across the activity classes. No major misclassifications are observed, and only a limited number of off-diagonal entries occur. These results further validate the effectiveness of the proposed feature extraction and selection technique in capturing highly discriminative representations for human activity recognition.

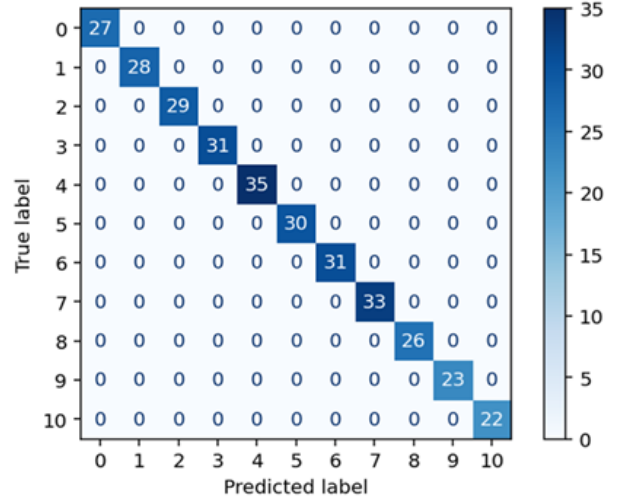
For clarity, the correspondence between the class indices (0–10) and their respective activity labels is given in Table 7. This consistent behaviour across SVM, Random Forest, KNN, and Logistic Regression highlights the effectiveness of the proposed feature extraction and selection technique in capturing highly discriminative representations for HAR.

5.4 Analysis of Memory Usage and Training Time

Table 8 provides a comparative view of memory usage and training time for different classifiers under various FS strategies. It can be observed that the proposed ADFSA technique consistently achieves lower memory consumption and faster training compared to traditional approaches such as PCA and

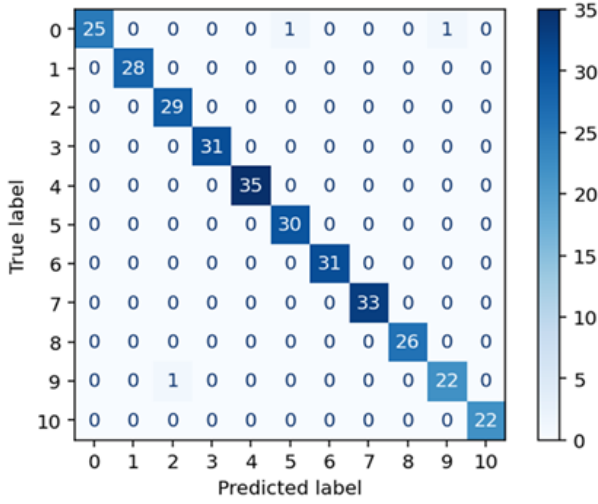


(a) SVM

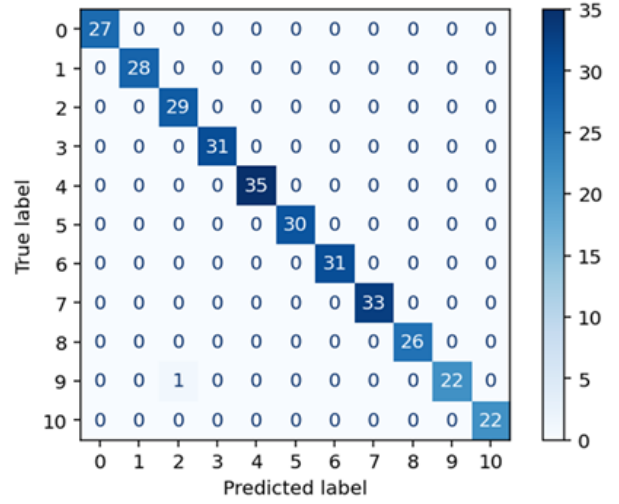


(b) Random Forest

Figure 14. Confusion Matrices of SVM and Random Forest



(a) KNN



(b) Logistic Regression

Figure 15. Confusion Matrices of KNN and Logistic Regression

Table 7. Class Activity Labels.

Index	Activity	Index	Activity
0	Basketball	6	Swing
1	Biking	7	Tennis Swing
2	Diving	8	Trampoline Jumping
3	Golf Swing	9	Volleyball Spiking
4	Horse Riding	10	Walking
5	Soccer Juggling		

RFE. For instance, SVM and Logistic Regression show a remarkable drop in both resource usage and training duration with ADFS, while KNN benefits significantly in terms of memory reduction. Although Random Forest maintains a similar memory footprint across methods, ADFS still contributes to a noticeable decrease in training time. Overall, the table highlights that the proposed technique offers a more efficient balance between memory usage and computational cost across diverse classifiers.

Table 9 highlights the impact of various FS techniques on memory consumption and training time across four classifiers. The baseline (No FS) represents the unaltered scenario, against which per-

Table 8. Memory usage and training time comparison for different FS methods across classifiers.

Classifier	Setting	Memory Used (KB)	Training Time (ms)
SVM	No FS	23.93	134
	PCA	11.04	36
	RFE	11.04	157
	ADFSA (Proposed)	3.65	5
RF	No FS	68.49	612
	PCA	68.52	581
	RFE	68.52	434
	ADFSA (Proposed)	68.49	227
KNN	No FS	717.2	3
	PCA	301.77	2
	RFE	301.77	2
	ADFSA (Proposed)	64.82	1
LogReg	No FS	24.28	516
	PCA	11.39	30
	RFE	11.39	30
	ADFSA (Proposed)	4.00	10

centage changes are compared. The proposed ADFSAs technique consistently demonstrates the most significant reductions in both memory usage and training time. For instance, in the case of SVM and KNN, ADFSAs achieves memory reductions of 84.75% and 90.96%, respectively, along with training time decreases exceeding 66%. Similarly, for LogReg, ADFSAs lowers memory usage by 83.53% and nearly eliminates training time (−98.06%), emphasizing its efficiency. In contrast, traditional methods such as PCA and RFE show mixed outcomes: although PCA significantly reduces memory and training time for most classifiers, it slightly increases memory usage in RF. RFE, while effective in reducing memory, results in increased training time in SVM and offers limited efficiency gains in other classifiers. These results reinforce the capability of ADFSAs to enhance resource efficiency, making it particularly suitable for real-time and resource-constrained machine learning environments.

Table 9. Percentage change (%) in memory usage and training time compared to the No FS baseline for each classifier

Classifier	Setting	Δ Memory (%)	Δ Training Time (%)
SVM	No FS	0.00	0.00
	PCA	−53.87	−73.13
	RFE	−53.87	+17.16
	ADFSAs (Proposed)	−84.75	−96.27
RF	No FS	0.00	0.00
	PCA	+0.04	−5.07
	RFE	+0.04	−29.08
	ADFSAs (Proposed)	0.00	−62.91
KNN	No FS	0.00	0.00
	PCA	−57.92	−33.33
	RFE	−57.92	−33.33
	ADFSAs (Proposed)	−90.96	−66.67
LogReg	No FS	0.00	0.00
	PCA	−53.09	−94.19
	RFE	−53.09	−94.19
	ADFSAs (Proposed)	−83.53	−98.06

The effectiveness of ADFSAs on memory usage and training time can be clearly seen from Figures 16 and Figure 17 of both the SVM and RF classifiers, respectively. The reduction in both memory usage and training time for the SVM classifier can be seen in Figure 16, about an 84.75% drop in memory and a 79.11% decrease in training time achieved by the proposed ADFSAs technique as compared to PCA and RFE. It is therefore observed that the unusability of RFE for the SVM classifier in this regard. In contrast, all the methods have nearly occupied constant memory across all techniques, but still proposed ADFSAs observing a decrease of 62.91% in training time, as compared to only 5.07% and

29.08% achieved by PCA and RFE, respectively. Overall, it is clearly observed that the robustness and efficacy of the proposed ADFSFA in terms of FS in real-time and computationally constrained environments.

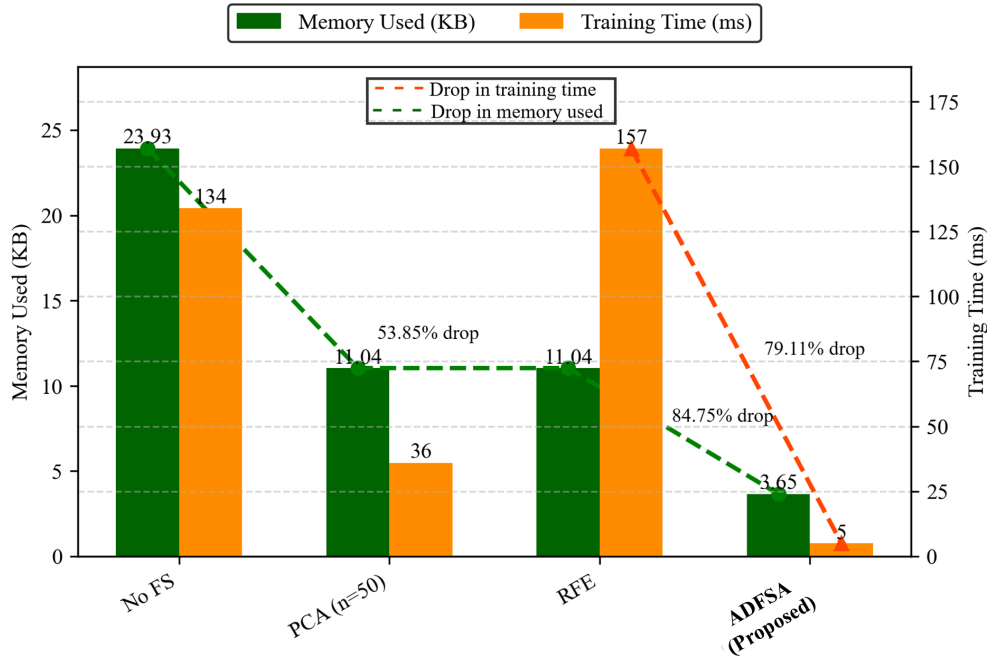


Figure 16. Memory vs Training-Time of SVM classifier using selective FS.

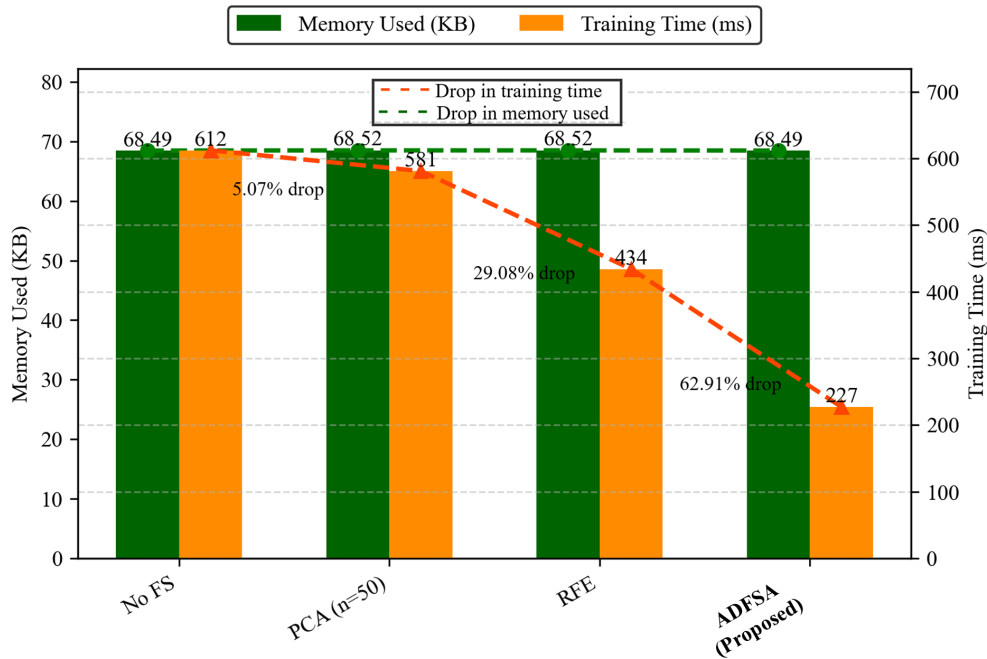


Figure 17. Memory vs Training-Time of RF classifier using selective FS.

FS techniques on KNN and LogReg are presented in Figure 18 and Figure 19, demonstrating the superiority of the proposed ADFSFA in terms of both training time and memory usage. Figure 18 shows the improvement in memory usage of the KNN classifier across all the adopted methods, including ADFSFA, having a dramatic reduction of about 90.96%, and training time by 66.67% for both RFE and PCA. The figure clearly demonstrates the moderate memory reduction of 57.92%, and a modest improvement in training time of about 33.33%. These observations clearly satisfy the ADFSFA as a

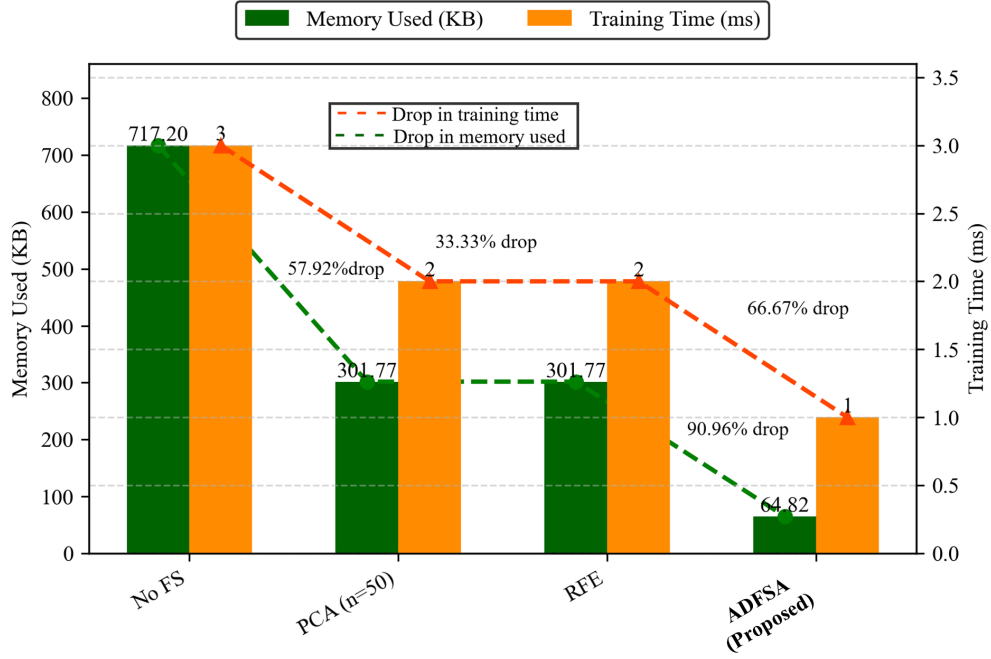


Figure 18. Memory vs Training-Time of KNN classifier using selective FS.

better option for KNN in memory-constrained or speed-sensitive applications. During observation

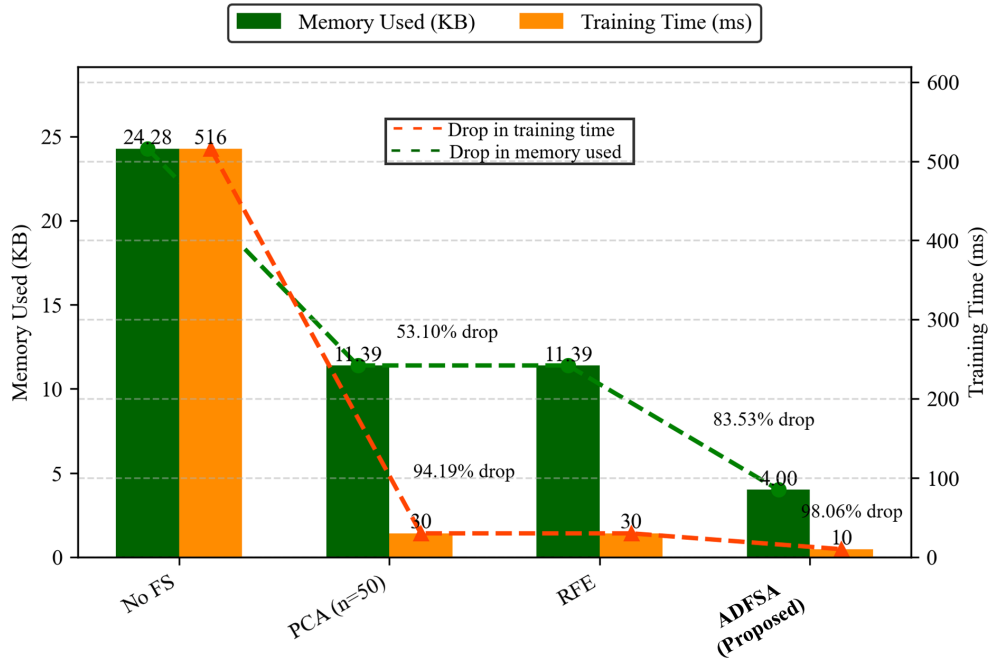


Figure 19. Memory vs Training-Time of LogReg classifier using selective FS.

of using the LogReg classifier, the proposed ADFS shows a better choice for memory-constrained devices, having a significant drop of about 83.53% of memory usage, and training time by an impressive 98.06%. By observing Figure 19, once again, the usability of ADFS in memory-constrained or speed-sensitive applications is proven.

5.5 Other Performance Matrices

Table 10 presents the comparative performance of four classifiers, SVM, RF, KNN, and LogReg across different FS strategies, namely no FS, PCA, RFE, and the proposed ADFSFA technique. For all classifiers, the proposed ADFSFA technique consistently achieved the highest F1-score, precision, and recall values, demonstrating a significant performance improvement over the baseline and conventional FS methods. Specifically, SVM reached an F1-score of 99.58%, RF attained 99.65%, KNN achieved 99.58%, and Logistic Regression obtained 99.51% with ADFSFA, surpassing other configurations by notable margins. In contrast, the No FS, PCA, and RFE settings showed relatively close but lower results, typically in the 97.2%–97.8% range for all metrics. These findings indicate that ADFSFA not only enhances classification accuracy but also maintains a balanced trade-off between precision and recall, highlighting its effectiveness in improving overall model performance.

Table 10. Proposed FS and other performance metrics.

Classifier	Setting	F1-score (%)	Precision (%)	Recall (%)
SVM	No FS	97.35	97.33	97.36
	PCA	97.79	97.75	97.78
	RFE	97.73	97.71	97.72
	ADFSFA (Proposed)	99.58	99.57	99.58
RF	No FS	97.23	97.21	97.23
	PCA	97.45	97.42	97.45
	RFE	97.51	97.48	97.51
	ADFSFA (Proposed)	99.65	99.62	99.65
KNN	No FS	97.32	97.29	97.32
	PCA	97.54	97.51	97.54
	RFE	97.44	97.40	97.44
	ADFSFA (Proposed)	99.58	99.54	99.58
LogReg	No FS	97.39	97.35	97.39
	PCA	97.58	97.55	97.58
	RFE	97.57	97.54	97.57
	ADFSFA (Proposed)	99.51	99.48	99.51

The statistical analysis for F1-score is summarized in Table 11, which reports the F1-scores with 95% confidence intervals and corresponding p -values for each classifier under different FS settings. The proposed ADFSFA technique consistently achieves the highest F1-scores across all classifiers, with values exceeding 99.5% and narrow confidence intervals, indicating superior accuracy and stability. In contrast, baseline configurations without FS, as well as PCA- and RFE-based approaches, yield F1-scores in the range of 97.2–97.8%, with differences statistically significant at $p < 0.001$. These results demonstrate the robustness and generalizability of ADFSFA in enhancing classification performance compared to conventional FS techniques.

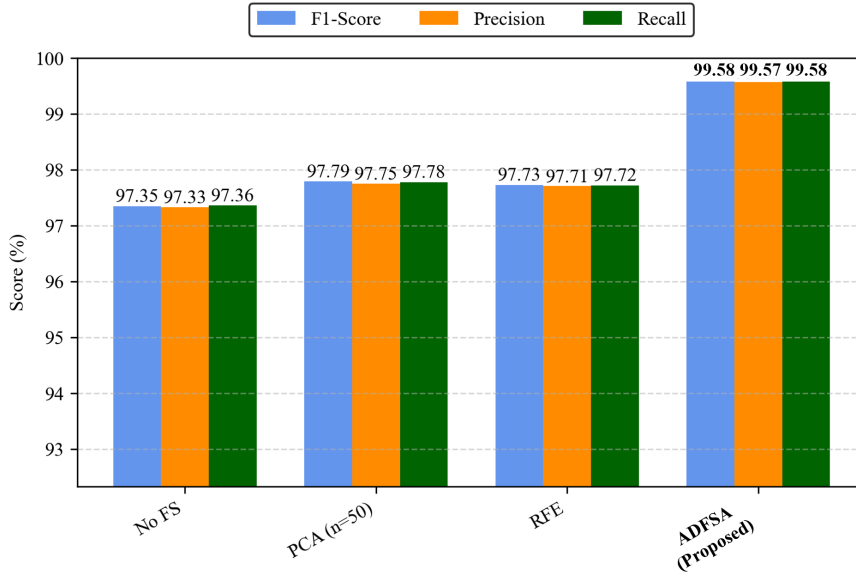
Furthermore, Figures 20–23 present a comparative analysis of the performance metrics, including F1-score, Precision, and Recall, for four classifiers: SVM, RF, KNN, and LogReg, respectively. Each figure includes grouped bar charts that visualize the impact of four FS methods: *No FS*, *PCA*, *RFE*, and the *proposed ADFSFA* technique.

The results clearly indicate that across all classifiers, the ADFSFA method consistently achieves the highest scores in all three evaluation metrics. For example, Figure 20 shows that SVM with ADFSFA reaches an F1-score of 99.58%, while Figure 21 highlights a similar peak of 99.65% for the RF classifier. The consistent upward trend across Figure 22 and Figure 23 further confirms the superiority of the ADFSFA method when applied to KNN and LogReg. These improvements across different learning algorithms demonstrate the robustness and generalizability of the proposed FS technique.

Overall, the analysis confirms that ADFSFA consistently enhances computational efficiency across diverse classifiers. Although traditional techniques like PCA and RFE contribute to some extent, they fail to achieve the balance between memory economy and training speed that ADFSFA provides. This reinforces the suitability of ADFSFA as a versatile FS strategy for scalable machine learning

Table 11. F1-score (%) with 95% confidence intervals and p-values vs ADFSFA (simulated data).

Classifier	Setting	F1-score (mean \pm CI)	p-value vs ADFSFA
SVM	No FS	97.35 \pm 0.24	< 0.001
	PCA	97.79 \pm 0.25	< 0.001
	RFE	97.73 \pm 0.27	< 0.001
	ADFSFA (Proposed)	99.58 \pm 0.21	—
RF	No FS	97.23 \pm 0.25	< 0.001
	PCA	97.45 \pm 0.25	< 0.001
	RFE	97.51 \pm 0.23	< 0.001
	ADFSFA (Proposed)	99.65 \pm 0.20	—
KNN	No FS	97.32 \pm 0.22	< 0.001
	PCA	97.54 \pm 0.26	< 0.001
	RFE	97.44 \pm 0.23	< 0.001
	ADFSFA (Proposed)	99.58 \pm 0.22	—
LogReg	No FS	97.39 \pm 0.26	< 0.001
	PCA	97.58 \pm 0.24	< 0.001
	RFE	97.57 \pm 0.26	< 0.001
	ADFSFA (Proposed)	99.51 \pm 0.21	—

**Figure 20.** Performance of SVM using different FS Methods.

pipelines.

5.6 Ablation Study

Figure 24 and Table 12 presents an ablation study conducted using the SVM classifier to evaluate the individual and combined effects of the uniqueness-based reward and complexity penalty in the proposed FS technique. Three configurations were tested: (i) *No Uniqueness, No Complexity Penalty*, (ii) *No Complexity Penalty*, and (iii) *Full* (both components enabled).

Table 12. Performance of SVM under various FS Strategies.

Classifier	Setting	CV Accuracy(%)	# Features	Avg Inf Time (ms)
SVM	No FS	97.35	128	1.242
	PCA	97.79	50	0.313
	RFE	97.73	50	0.468
	Proposed Techniques			
	No Uniq. No Comp. Penalty	98.23	52	0.250
	No Complexity Penalty	98.75	64	0.330
	Ensemble (Full)	99.58	7	0.190

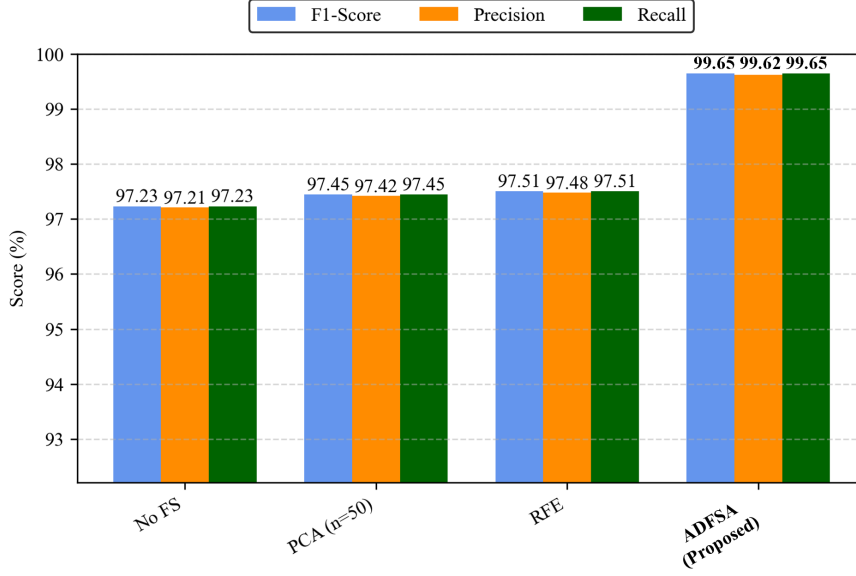


Figure 21. Performance of RF using different FS Methods.

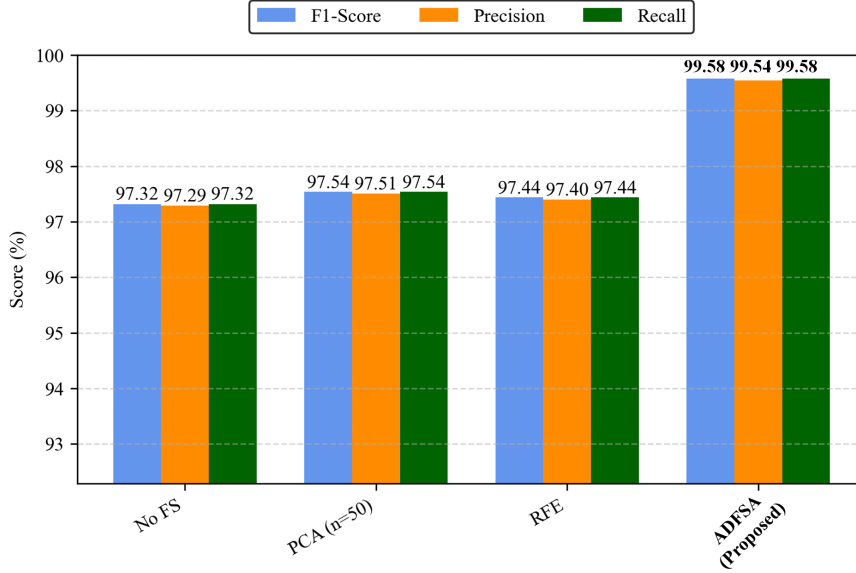


Figure 22. Performance of KNN using different FS Methods.

In the absence of both mechanisms, the model achieved a cross-validation (CV) accuracy of 98.23% with 52 selected features and an average inference time of 0.25 ms. When only the complexity penalty was removed, the number of features increased to 64, and the inference time rose to 0.33 ms, with a marginal accuracy improvement to 98.75%. In contrast, the *Full* configuration, which applies both uniqueness-driven exploration and complexity-aware reduction, yielded the highest CV accuracy of 99.58% with only 7 features and the lowest inference time of 0.19 ms.

These results clearly demonstrate that the combined application of the uniqueness reward and complexity penalty not only enhances model accuracy but also promotes feature compactness and efficiency, leading to faster inference and reduced model complexity.

Figure 25 and 26 illustrates the impact of different fitness function configurations on the optimizer’s weight update behavior and FS performance. In the first setting, Fig. 25a, where neither uniqueness nor complexity penalties are applied, the optimizer enters a stagnation phase after just 6 generations, resulting in the selection of 52 features. This early stagnation indicates poor exploration capability

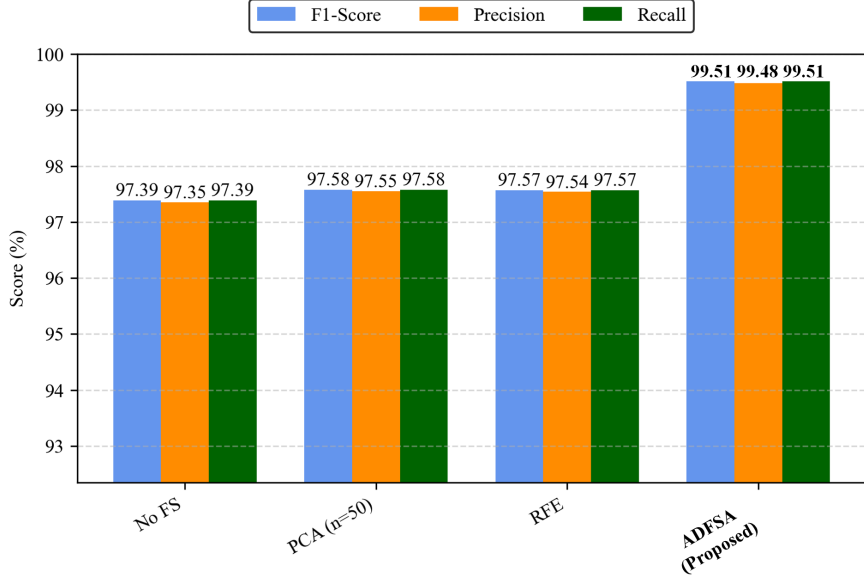


Figure 23. Performance of LogReg using different FS methods.

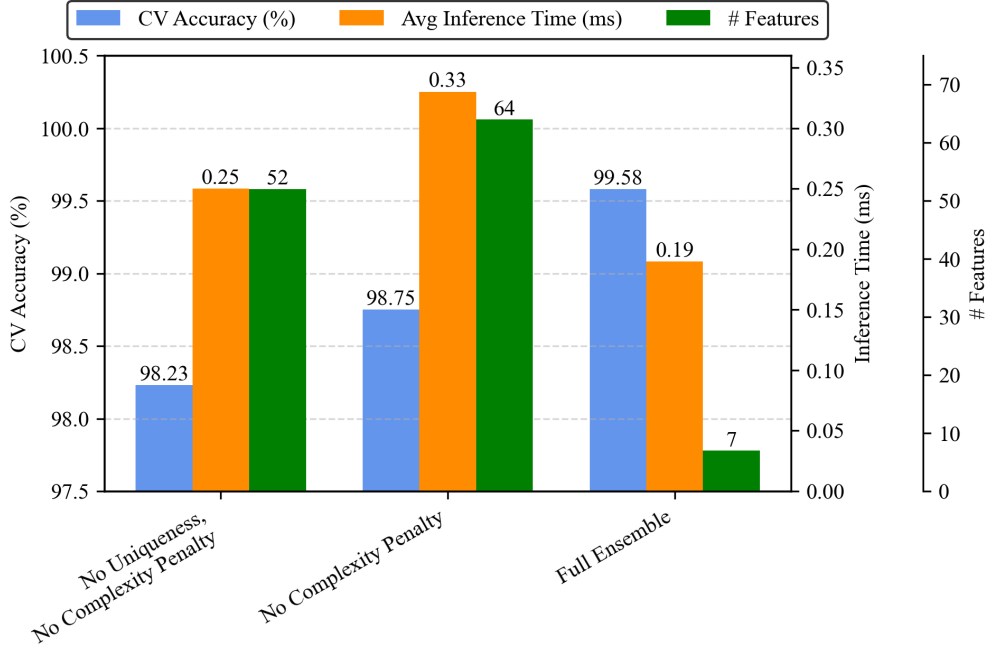
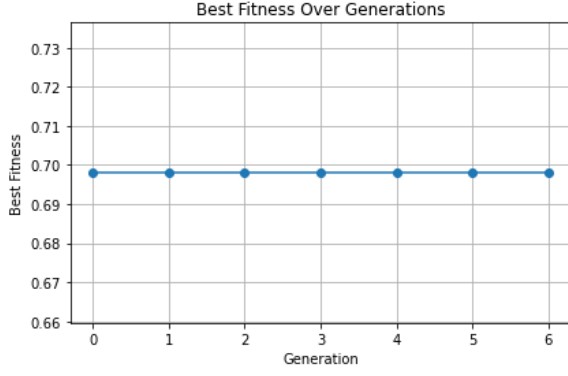
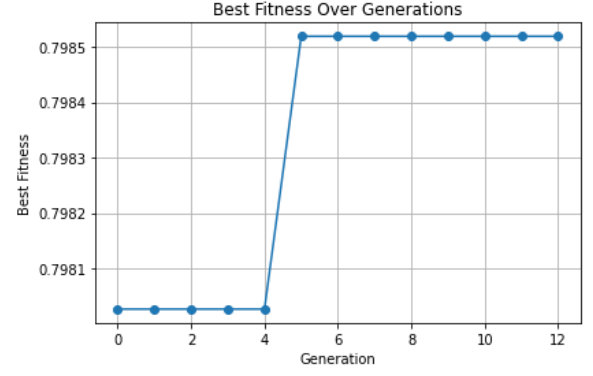


Figure 24. Ablation study on SVM classifier

and a tendency to converge prematurely. In the second configuration, Fig. 25b, which includes only the complexity penalty, the optimizer shows a modest improvement by stagnating after 12 generations and selecting 64 features, suggesting some control over model complexity but still lacking diversity in the solution space. In contrast, the third configuration, Fig. 26 uses the complete fitness function with both uniqueness and complexity components. This setup allows the optimizer to utilize the full range of generations without premature stagnation and leads to a significantly reduced and optimal feature subset of only 7 features. These results demonstrate the importance of balancing exploration and exploitation through well-designed fitness objectives in FS tasks.



(a) No uniq. and compl. penalty



(b) No complexity penalty

Figure 25. Impact of different components of the fitness function on FS performance.

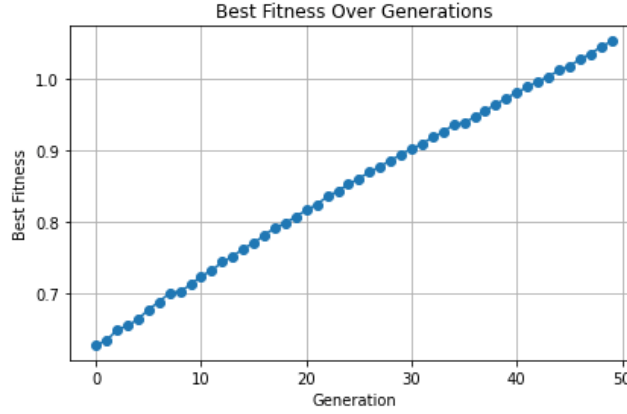


Figure 26. Fitness function with full configuration

5.7 Comparison of Proposed Framework with the State Of The Art

Table 13 summarizes a broad spectrum of representative deep learning methods evaluated on the UCF-YouTube dataset. Earlier frameworks, such as CNN-BiLSTM [13] and Deep Autoencoder+CNN [14], obtained 92.84% and 96.2% recognition accuracy, respectively, but were largely tailored for static spatial information and lacked explicit modeling of long-term temporal dependencies. Subsequent works attempted to address this issue by combining convolutional architectures with recurrent networks. For example, the Dilated CNN+BiLSTM+RB [16] and Local-Global features+QSVM [17] frameworks achieved 89.01% and 82.6%, respectively, under a 70/30 train-test split. Although these approaches improved temporal modeling, their performance remains moderate, suggesting limited scalability to highly dynamic human activity sequences.

Table 13. Comparison of classification accuracy using different models on the UCF-YouTube dataset

Method	Year	Split Ratio (Train/Val/Test)	Accuracy (%)
CNN-BiLSTM [13]	2018	60/20/20	92.84
Deep autoencoder+CNN [14]	2019	—	96.2
KFDI [15]	2020	—	79.4
Dilated CNN+BiLSTM+RB [16]	2021	70 (train)/ 30 (test)	89.01
Local-global features+QSVM [17]	2021	70 (train)/ 30 (test)	82.6
3DCNN [18]	2022	70/10/20	85.20
VGG-BiGRU [20]	2023	60/20/20	93.38
ViT-ReT [21]	2023	80 (train)/20 (test)	92.4
A bidirectional LSTM model [22]	2024	80 (train)/20 (test)	99.2
ConvNeXt-TCN [19]	2025	70/10/20	97.73
Proposed	2025	80 (train)/20 (test)	99.58

Recent transformer-based and hybrid models have further improved spatial-temporal learning; for example, ViT-ReT [21], 3DCNN [18], and VGG-BiGRU [20] achieved 92.4%, 85.20%, and 93.38% accuracy, respectively. More advanced approaches, such as the 2024 bidirectional LSTM [22] and ConvNeXt-TCN [19], reported 99.2% and 97.73%. By comparison, the proposed framework yields a higher accuracy of 99.58% on the same 80/20 split by effectively integrating spatial-temporal feature learning with an optimized FS strategy, demonstrating strong generalization and suitability for real-time HAR applications.

6 Conclusion and Future Work

This work proposes a hybrid deep learning framework for solving real-time problems in video-based HAR, such as cluttered backgrounds, poor illumination, and irrelevant information. Inception-V3 is customized in such a way as to remove the aforementioned problems by incorporating average pooling and max pooling layers. This customized inceptionV3 model is trained using a transfer learning technique. After training, the head is removed, and spatial-domain features are extracted using this customized and trained InceptionV3 model. These spatial-domain features are fed into the AA-LSTM network for training using 20 series sequences to learn temporal-domain information. At this stage, the features are now rich in spatial and temporal information. These features are further processed through the proposed ADFSFA technique for obtaining a compact with no information loss. Compared to conventional dimensionality reduction methods such as PCA and RFE, the proposed ADFSFA technique consistently achieved better classification performance. This improvement was observed across multiple machine-learning classifiers, including SVM, Random Forest, KNN, and Logistic Regression. ADFSFA reduced the feature set from 128 to only 7 features and boosted cross-validation accuracy to above 99.5%, outperforming PCA and RFE by more than 1.7% on average. This drastic feature reduction also translated into significant gains in computational efficiency. Inference time was decreased by up to 84% (e.g., from 1.24 ms to 0.20 ms in SVM), training times were accelerated by factors ranging from $3\times$ to over $25\times$ depending on the classifier. Additionally, memory consumption was minimized to as low as 3.65 KB in SVM models. These results demonstrate that ADFSFA enhances classification accuracy, improving training speed, lowering the inference latency, and minimizing memory usage. All mentioned characteristics make the proposed ADFSFA suitable for scalable, real-time HAR applications on resource-constrained devices. The proposed technique effectively balances model complexity and predictive performance, validating its potential as a robust FS framework for video-based HAR systems.

Future work will focus on leveraging self-supervised learning techniques for human activity recognition to minimize dependence on labeled datasets. Transformer-based temporal modeling will be investigated as a potential replacement for LSTM networks to enhance the capture of long-range motion dependencies. The proposed framework will also be adapted for deployment on low-power edge devices, such as the Raspberry Pi, to evaluate its real-time performance in resource-constrained settings. Furthermore, the methodology will be validated on more diverse and challenging video datasets, including HMDB51, to rigorously assess its generalization across a broad spectrum of activity categories and environmental conditions.

References

- [1] A. Ullah, K. Muhammad, W. Ding, V. Palade, I. U. Haq, S. W. Baik, "Efficient activity recognition using lightweight CNN and DS-GRU network for surveillance applications", *Applied Soft Computing*, Volume 103, 2021, 107102, ISSN 1568-4946, <https://doi.org/10.1016/j.asoc.2021.107102>.
- [2] Morshed, M. G., Sultana, T., Alam, A., & Lee, Y.-K. (2023). Human Action Recognition: A Taxonomy-Based Survey, Updates, and Opportunities. *Sensors*, 23(4), 2182. <https://doi.org/10.3390/s23042182>.
- [3] K. Simonyan, A. Zisserman, Two-stream convolutional networks for action recognition in videos, in: *Advances in Neural Information Processing Systems*, 2014, pp. 568–576.
- [4] Y. Shi, Y. Tian, Y. Wang, T. Huang, Sequential deep trajectory descriptor for action recognition with three-stream CNN, *IEEE Trans. Multimed.* 19 (7) (2017) 1510–1520.
- [5] D. Tran, L. Bourdev, R. Fergus, L. Torresani and M. Paluri, "Learning Spatiotemporal Features with 3D Convolutional Networks," 2015 IEEE International Conference on Computer Vision (ICCV), Santiago, Chile, 2015, pp. 4489-4497, doi: 10.1109/ICCV.2015.510. and Pattern Recognition (CVPR); 2021 Jun 20–25; Nashville, TN, USA. p. 3156–64.
- [6] X. Wang, L. Gao, P. Wang, X. Sun, X. Liu, Two-stream 3-D convnet fusion for action recognition in videos with arbitrary size and length, *IEEE Trans. Multimed.* 20 (3) (2017) 634–644.
- [7] R. Zhao, H. Ali and P. van der Smagt, "Two-stream RNN/CNN for action recognition in 3D videos," 2017 IEEE/RSJ International Conference on Intelligent Robots and Systems (IROS), Vancouver, BC, Canada, 2017, pp. 4260-4267, doi: 10.1109/IROS.2017.8206288.
- [8] M. Majd, R. Safabakhsh, "Correlational convolutional LSTM for human action recognition", *Neurocomputing* 396, (2020) 224–229.
- [9] Liu, M., Li, W., He, B., Wang, C., & Qu, L. (2025). "Human Action Recognition Based on 3D Convolution and Multi-Attention Transformer." *Applied Sciences*, 15(5), 2695. <https://doi.org/10.3390/app15052695>
- [10] Guo, X., Kim, Y., Ning, X., & Min, S. D. (2025). "Enhancing the Transformer Model with a Convolutional Feature Extractor Block and Vector-Based Relative Position Embedding for Human Activity Recognition." *Sensors*, 25(2), 301. <https://doi.org/10.3390/s25020301>
- [11] H. Zhang, Z. Zhuang, X. Wang, X. Yang, and Y. Zhang, "MoPFormer: Motion-Primitive Transformer for Wearable-Sensor Activity Recognition," *arXiv preprint arXiv:2505.20744*, submitted May 2025.
- [12] Y. Liu, X. Qin, Y. Gao, X. Li, and C. Feng, "SETransformer: A Hybrid Attention-Based Architecture for Robust Human Activity Recognition," **arXiv preprint arXiv:2505.19369**, May 2025.
- [13] H. Shahverdi and S. A. Ghorashi, "Lightweight Transformer for Robust Human Activity Recognition Using Smartphone IMU Data," in **Proc. 14th International Conference on Human Interaction and Emerging Technologies: Artificial Intelligence & Future Applications (IHET-FS 2025)**, London, UK, Jun. 2025.
- [14] C. S. Leite, H. Mauranen, A. Zhanabatyrova, and Y. Xiao, "Transformer-Based Approaches for Sensor-Based Human Activity Recognition: Opportunities and Challenges," **arXiv preprint arXiv:2410.13605**, Oct. 2024.

- [15] F. Afza, M. A. Khan, M. Sharif, S. Kadry, G. Manogaran, T. Saba, I. Ashraf, R. Damaševičius, A framework of human action recognition using length control features fusion and weighted entropy-variances based feature selection, *Image and Vision Computing*, Volume 106, 2021, 104090, ISSN 0262-8856, <https://doi.org/10.1016/j.imavis.2020.104090>.
- [16] M. A. Khan, K. Javed, S. A. Khan, T. Saba, U. Habib, J. A. Khan and A. A. Abbasi, "Human action recognition using fusion of multiview and deep features: an application to video surveillance," *Multimed Tools Applications*, vol. 83, no. 5, p. 14885–14911, 2020.
- [17] J. Liu, J. Luo and M. Shah, Recognizing Realistic Actions from Videos "in the Wild", *IEEE International Conference on Computer Vision and Pattern Recognition(CVPR)*, 2009.
- [18] Ye, J.; Wang, L.; Li, G.; Chen, D.; Zhe, S.; Chu, X.; Xu, Z. Learning compact recurrent neural networks with block-term tensor decomposition. In *Proceedings of the IEEE Conference on Computer Vision and Pattern Recognition*, Alt Lake City, UT, USA, 18–22 June 2018; pp. 9378–9387.
- [19] Ullah A, Ahmad J, Muhammad K, Sajjad M, Baik SW. Action recognition in video sequences using deep bi-directional LSTM with CNN features. *IEEE Access*. 2018;6:1155–66. <https://doi.org/10.1109/ACCESS.2017.2778011>.
- [20] Ullah, A.; Muhammad, K.; Haq, I.U.; Baik, S.W. Action recognition using optimized deep autoencoder and CNN for surveillance data streams of non-stationary environments. *Future Gener. Comput. Syst*. 2019, 96, 386–397.
- [21] Riahi, M., Eslami, M., Safavi, S.H. and Torkamani Azar, F. (2020), Human activity recognition using improved dynamic image. *IET Image Process.*, 14: 3223–3231. <https://doi.org/10.1049/iet-ipr.2019.1739>.
- [22] Muhammad, K.; Ullah, A.; Imran, A.S.; Sajjad, M.; Kiran, M.S.; Sannino, G.; de Albuquerque, V.H.C. Human action recognition using attention based LSTM network with dilated CNN features. *Future Gener. Comput. Syst*. 2021, 125, 820–830.
- [23] Al-Obaidi, S.; Al-Khafaji, H.; Abhayaratne, C. Making sense of neuromorphic event data for human action recognition. *IEEE Access* 2021, 9, 82686–82700.
- [24] Vrskova R, Hudec R, Kamencay P, Sykora P. Human activity classification using the 3DCNN architecture. *ApplSci*. 2022;12(2):931. doi:10.3390/app12020931.
- [25] J. Shin, M.A.M. Hasan, M. Maniruzzaman, S. Nishimura, and S. Alfarhood, "Video-Based Human Activity Recognition Using Hybrid Deep Learning Model," *Comput. Model. Eng. Sci.*, vol. 143, no. 3, pp. 3615–3638, 2025. <https://doi.org/10.32604/cmes.2025.064588>.
- [26] Ahmad T, Wu J, Alwageed HS, Khan F, Khan J, Lee Y. Human activity recognition based on deep-temporal learning using convolution neural networks features and bidirectional gated recurrent unit with features selection. *IEEE Access*. 2023;11:33148–33159. <https://doi.org/10.1109/ACCESS.2023.3263155>.
- [27] Wensel J, Ullah H, Munir A. ViT-ReT: vision and recurrent transformer neural networks for human activity recognition in videos. *IEEE Access*. 2023;11:72227–72249. <https://doi.org/10.1109/ACCESS.2023.3293813>.
- [28] Hassan, N.; Miah, A.S.M.; Shin, J. A Deep Bidirectional LSTM Model Enhanced by Transfer-Learning-Based Feature Extraction for Dynamic Human Activity Recognition. *Appl. Sci*. 2024, 14, 603. <https://doi.org/10.3390/app14020603>.
- [29] N. Cauli, & D. Reforgiato Recupero, (2022). Survey on Videos Data Augmentation for Deep Learning Models. *Future Internet*, 14(3), 93. <https://doi.org/10.3390/fi14030093>

- [30] M. A. Arshad et al., "Drone Navigation Using Region and Edge Exploitation-Based Deep CNN," in *IEEE Access*, vol. 10, pp. 95441-95450, 2022, doi: 10.1109/ACCESS.2022.3204876.
- [31] A. Mehmood, Y. Hu, and S. H. Khan, "A Novel Channel Boosted Residual CNN-Transformer with Regional-Boundary Learning for Breast Cancer Detection," *arXiv preprint arXiv:2503.15008*, Mar. 2025.
- [32] Khan, S.H.; Sohail, A.; Khan, A.; Lee, Y.-S. COVID-19 Detection in Chest X-ray Images Using a New Channel Boosted CNN. *Diagnostics* 2022, 12, 267. <https://doi.org/10.3390/diagnostics12020267>
- [33] A. Maćkiewicz, W. Ratajczak "Principal components analysis (PCA)" *Computers and Geosciences*, Volume 19, Issue 3, 1993
- [34] X. -w. Chen and J. C. Jeong, "Enhanced recursive feature elimination," *Sixth International Conference on Machine Learning and Applications (ICMLA 2007)*, Cincinnati, OH, USA, 2007, pp. 429-435, doi: 10.1109/ICMLA.2007.35.
- [35] A. D. Cioppa, C. D. Stefano and A. Marcelli, "Where Are the Niches? Dynamic Fitness Sharing," *IEEE Transactions on Evolutionary Computation* , vol. 11, no. 4, pp. 453 - 465, 2007.